# NANOPARTICLES-BASED MAGNETIC AND PHOTO INDUCED HYPERTHERMIA FOR CANCER TREATMENT

S. K. Sharma[1], Navadeep Shrivastava[2], F. Rossi[3,4,5], L. D. Tung[3,4] and N. T. K. Thanh[3,4*]

[1]Department of Physics, Faculty of Science & Technology, The University of the West Indies, St. Augustine, Trinidad and Tobago.
[2]Institute of Physics, Federal University of Goiás, Goiânia - GO, Brazil.
[3]Biophysics Group, Department of Physics & Astronomy, University College London, Gower Street, LondonWC1E 6BT, UK.
[4]UCL Healthcare Biomagnetic and Nanomaterials Laboratory, 21 Albemarle Street, London W1S 4BS, UK.
[5]A*STAR, IMRE, Kinesis 11th floor, Fusionopolis 2, 138635, Singapore.

***E-MAIL:** ntk.thanh@ucl.ac.uk

## Table of Content

**Abstract**

Nanoscience provides several modalities to combat cancer disease effectively. Magnetic hyperthermia and photothermal therapy techniques are central research themes among various groups in the world by utilizing magnetic and optical characteristics of distinct or composite nanoentities. This review provides the current research on both the techniques and their successes towards clinical translation. The review discusses about the various heating mechanisms involved in magnetic and photo-induced hyperthermia. We have evaluated potential functional nanoparticles with excellent properties capable of providing innovative future solutions to current problems associated with these therapies. Several factors (extracellular and intracellular) have been covered and explained which may affect such thermal treatments. We have provided some instrumental and technical details of both the techniques that are important for consideration in using these modalities of treatments. A direct comparison of these two techniques and a further need of the combined therapy (magnetic hyperthermia plus photothermal therapy) was highlighted as a new pathway for cancer treatments.

**Keywords:** Nanoparticles; Magnetic and photothermal hyperthermia; Combined “Mag-Photo” therapy; Biodistribition; Clinical treatment.

## 1. Introduction

Temperature is one of the basic variables in science and with the latest advancements in nanothermometry nowadays it can be measured with submicrometric spatial resolution [1]. The resolution in temperature measurements expands the applications and control of temperature changes in biological systems leading to a detailed determination of their dynamics and viability for a wide range of organic systems from cells, tissues to organisms [2]. The use of heat for the purpose of therapy is an old fashion methodology in ancient history which had a rise of popularity through the $19^{th}$ century as a treatment against cancer, being optimized in $21^{st}$ century, but still remained unaccomplished due to the lack of measuring methodologies [3]. In recent decades of "the nanoscale era", the research activities in terms of scientific/technological output using thermal treatments have led to renewed interest in thermal therapy, especially on the magnetic-thermal therapy and photo-induced thermal therapy [4]. Novel techniques for controlled and localized heat generation, monitoring it, and transferring localized heat to the biological targets are being proposed purposely and specified. The understanding of different mechanisms causing temperature induced cell killing, cell-modification and the capability to produce heat in the vicinity of cells is very important. The type of nanoscale materials used to generate heat from external force such as magnetic field, infrared (IR) radiation, X-rays etc., are the main focus of research in the field [5]. The basic mechanism of thermal therapy is sometime controversial due to a lack of comprehensive understanding of the local effects caused by the temperature elevation on individual cells in most of the given bio-specimen [6]. All thermal treatments are based on driving part of the

body or the whole above its normal temperature for a defined period of time. Temperature rise at cellular level causes changes in tissue elasticity, blood flow rate, protein synthesis, dissociation and inactivity of cells from minutes to several hours or days. The essential points in using thermal treatment are: the amount of localized temperature rise in biosystems and the duration of treatment in external field force. The magnitude of the temperature gradient is the primary factor that classifies thermal treatments and their macroscopic effects on cancer cells/tumors in three major categories:

(1) **Diathermic treatment**: It is based on heating tissues and organs from the standard body temperature up to 41 $^{o}$C. These processes increase blood flow and cause a rise in the diffusion rates of "bio-liquids" across cell membranes but generally preserve the cellular homeostasis [6].

(2) **Hyperthermia Treatment (HT)**: It is required the local generation of temperature in the range from 41 to 48 $^{o}$C which is generally described as clinically relevant [7]. A comprehensive understanding of the biomechanisms acting at the cellular level in this range of temperature is still far from completion. In this temperature range, because of protein denaturation, aggregation and the synthesis of heat-shock proteins, long time treatments may lead to long term cell inactivation and change in the rates of several biochemical reactions. Hyperthermia treatments commonly used in combination with other cancer treatments such as chemotherapy or radiation therapy which are applied after due to increased susceptibility to the treatments of the heat stressed cells [8].

(3) **Irreversible thermal treatment**: It includes all treatments that increase the tumor temperature above 48 $^{o}$C for a relatively short time. At this temperature range the

effect on cells/tissues is drastic and non-reversible [9]. Irreversible thermal treatments can be very efficient in the ablation of tumors but sometimes they may cause secondary damages to DNA and proteins of healthy cells. So far that irreversible thermal treatments are not generally used for cancer treatment but primarily only in urology and cardiology as option to the traditional surgery [10].

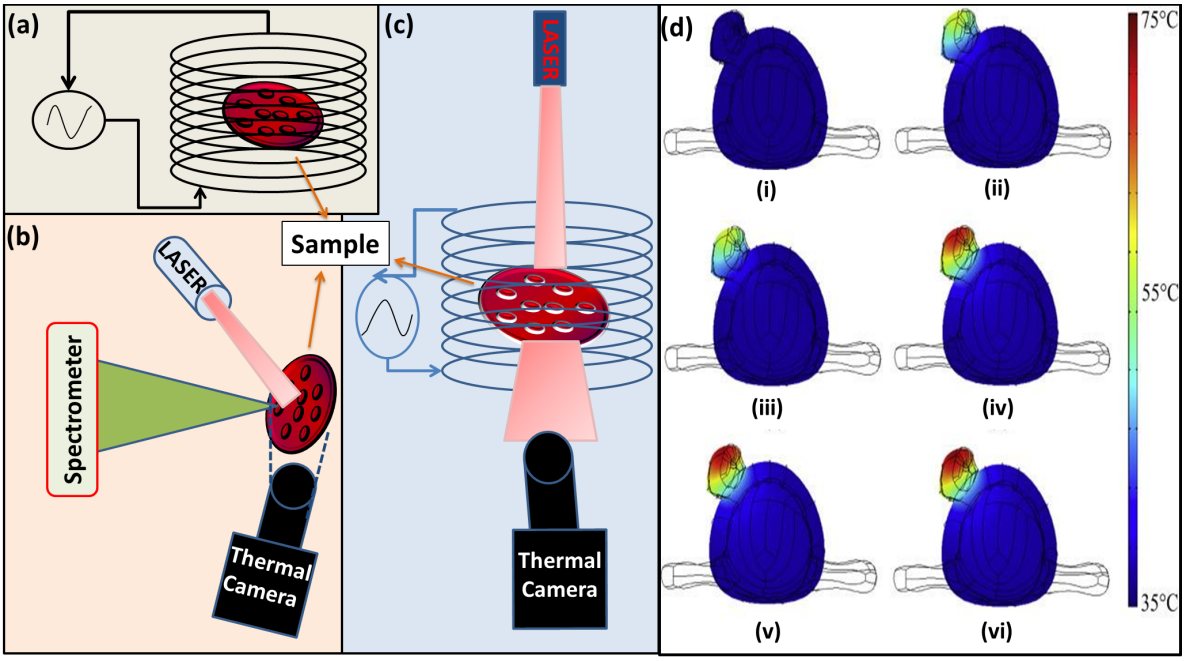


**Fig. 1:** Fundamental scheme of the experimental device setup for (a) magnetic hyperthermia treatment (MHT), (b) photothermal hyperthermia and (c) combined thermal therapy experiments. The temperature increase can be recorded with an IR thermal imaging camera located at the end of the coil cavity or fiber-optical thermometer. (d) Slices of the temperature fields in the tumor and mouse body obtained using COMSOL software [11]: i) before heating, ii) 3 min, iii) 6 min, iv) 9 min, v) 12 min, and vi) 15 min after the heating starts. Note that the steady-state temperature field is established after 15 min. (Reprinted with permission from Ref. [11]. Copyright 2016, Elsevier Ltd).

Besides direct thermal-induced therapy, there are several other techniques and methodologies which contribute to the efficiency of hyperthermia as a therapeutic tool against cancer diseases such as oxygenation, pH-maintenance, photodynamic therapy, heat released chemotherapy, etc. [7]. Compared with others, thermal therapy is less invasive, and it increases the efficacy of traditional treatments by reducing side effects. Using a sufficiently accurate control, thermal therapy has been used for localized heating of cancer cells with minimal effect on normal cells [12]. Heating on superficial tumors can be done using radio frequencies, microwave irradiation, ultrasound techniques or with IR laser sources [13]. Depending on the depth and size of cancerous tissue, several parameters in instrumental setup can be varied in order to get a more effective treatment. Figs. 1a &1b explain the fundamental experimental arrangements of the magnetic hyperthermia treatment (MHT) as well as the photothermal treatment (PTT) and they can be combined together (Fig. 1c) for more effective treatments [14].

In difference with micro or bulk counterparts, materials synthesized and engineered on nanoscale usually have novel characteristics which may be favorable in biological systems for interaction with cell surface and intercellular structures. Nowadays the nanoscale materials have become strong candidates for medical treatments as carriers for drugs, therapy and for the detection of diseases. In cancer or tumor treatment, nanoparticles (NPs) have recently been considered as a promising new approach [15]. Nanomedicine requires a multidisciplinary attitude and its understanding requiring knowledge of ethical, physical, chemical, physiological and biological aspects. Nanotechnology promises to revolutionize the area of cancer/tumor treatment with a wide spectrum of nanostructures including polymers, dendrimers, lipids, organometallic, carbon based materials, several inorganic nanomaterials (iron oxide, Au, Ag,

semiconductor quantum dots- QDs) contributing to development of treatments with different physical process and mechanisms of action [15]. An approach to the selection of nanomaterials should consider biodistribution, toxicity (short and long term), size control, surface chemistry, their behavior in biological systems and the use of nanomaterials with their unique properties can open a new set of opportunity for medicine. Here, NPs can have therapeutic as well as diagnostic properties to be designed to carry a large therapeutic "payload" [4]. They can also be modified with targeting ligands which yield high affinity and specificity for target cells to deliver highly active chemotherapy and hyperthermia with cellular precision. The complex structure of NPs can be made to accommodate multiple active molecules simultaneously allowing combinatorial cancer therapy with different drugs [16] and biomimetic NPs can bypass cellular membranes as well as overcome drug resistance mechanism [17, 18]. Currently, NPs and nanoparticulate formulations have been integrated into cancer therapeutics and ongoing clinical trials with improved efficacy and reduced toxicity [19].

Thermal treatments mediated with nanomaterials can be classified through the process used to generate the therapeutic effect a slight activated in the photothermal and photodynamic therapies or magnetically induced for the magnetothermal therapy [18, 20]. Magnetothermal therapy is based on different mechanisms including hysteresis loss, Neel relaxation and Brown relaxation to convert the energy of an external magnetic field into heat. A typical method of delivering the NPs to the tumor site is the direct injection in the tumor area followed by diffusion in the damaged tissues [21]. The first clinical results in the field of MHT were obtained by Jordan *et al.* [22] against brain tumor using superparamagnetic iron-oxide coated by aminosilane. A benefit of using magnetic nanostructures for MHT is the simultaneously use of

either being contrast agent in magnetic resonance imaging (MRI) or acting as heat source when exposed to specific frequencies. On the negative side, MHT may cause protein denaturation, DNA damage, signaling interruption, cell growth inhibition and apoptosis [23].

PTT, or optical hyperthermia, uses the energy of laser to trigger the action of either photothermal conversion agents or specific physical phenomena to generate heat causing thermal ablation of cancer cells [24]. A field of PTT study has expanded since the beginning of the millennia with the development of easily producible Au nanostructures (*e.g.*, rods, cubes) [25], and nowadays it is extended to nanostructures with a variety of different elements or materials. Nanomaterials used in PTT are generally characterized by a great efficiency in photothermal conversion for wavelength in the near infrared (NIR) to exploit the optical window of living tissues [26]. In addition, the materials also need to have high performance, especially when applied to *in vivo*, a low toxicity and tumor targeting properties. NIR lasers are the main energy source for PTT which can penetrate through the tissues and be converted into heat by the nanomaterials (Fig. 1). Using laser directly to ablate tumor tissues would require high energy settings causing unintended damage to normal tissues. The introduction of a photothermal conversion agents allows the use of low energy laser able to penetrate healthy tissues without causing heat damages [16]. Several necessary characteristics are important for such agents including photostability, biocompatibility, large absorption coefficient and NIR absorption. Metals have different optical properties from standard dielectric materials (based on oxides, fluorides, nitrides etc.) and among them nanostructured Au is the most promising photothermal metallic agent. Here, the heating mainly involves surface plasmon generation or localized surface plasmon resonance from the interaction of light with metals. One of the

traditional draw backs of PTT was the necessity of the laser to be able to penetrate the healthy tissues without damaging them or loosing too much power (due to scattering).This limitation has been recently overcome by moving the light source inside the patient with the use of fiber optic waveguides. With a powerful laser source, the output, however, was relatively weak limited from fraction of watt to few watts for direct laser ablation or even lower for longer time when used for particles mediated hyperthermia [28].

The difference between MHT and PTT is the attainable tissue penetration. PTT is only able to treat tumors seated at the surface or a few millimeters below the tissue level because of limited tissue penetration of light [29] while MHT can treat tumors seated at any depth thanks to the large tissue penetration ability of the magnetic field [30]. Moreover, the contactless use of alternating ac magnetic field enables a controllable remote treatment to eliminate tumors that are inaccessible by PTT. The continuous effort of working on the subject of cancer treatments using thermal approach has been linked specially with the synthesis of nanomaterials focusing on high degree of shape-size tunability, surface modifications and bioconjugations with NPs. At the moment, a very few clinical centers use MHT/PTT for anticancer therapy, but there are a large number of particles and protocols in pre-clinical or in the process of being approved in Europe and USA for clinical use [31, 32]. The pursuit of innovative, multifunctional, more efficient and safer treatments is a major challenge in preclinical NP-mediated thermotherapeutic research, and it is important to search for “dual” materials to act as both magnetic and photothermal agents. In this review, we are aiming to provide comprehensive information about magnetic and photothermal hyperthermia including the processes involved in their mechanisms, on the factors affecting the efficiency, the

biological interactions as well as details on the instrumentations used for the therapies. We also review both the therapies at clinical levels and the combined therapy showing the research work on this hot topic.

## 2. Magnetic-induced hyperthermia

The primary target of hyperthermia is to deliver heat to kill cancerous cells at clinically adequate temperatures and to limit the damage to healthy tissue. Nanotechnology has provided a novel and original solution allows targeting regions in the body otherwise difficult to reach and thanks to their nanoscale design they open the possibility to conjugate biomolecules like antibodies for a more effective therapy or to accomplish specific targeting [33]. Magnetic-induced hyperthermia is minimally invasive, tissue-specific and capable of precisely localized and high-intensity heating in deep tissues. By heating the NPs using an external ac magnetic field, it is possible to improve the localization and deliver the heat into the tumor tissue [34]. The concept of magnetic materials used for hyperthermia applications was introduced by Gilchrist *et al.* [35] in 1957 and expanded in the mid-1990s thanks to the introduction of NPs. This resolved the difficulties occurring with radio frequencies related to power absorption of tissue for the cancer treatment which can overcome the difficulty to adjust to the variability of power absorption of cancerous tissues. Since the synthesis have great impact on the magnetic properties, it is fundamental to find appropriate synthetic methods with the ability to rigorously control the composition, size and shape of magnetic NPs (MNPs).

The heat efficiency generated by MNPs (fluids) is quantified by specific absorption rate (SAR) or specific loss power (SLP) and it is defined as the amount of heat released by an unitary amount

of active material per unit time during exposure to an ac magnetic field of defined frequency and field strength [23].

$$SAR = \mathrm{C}(\Delta T/\Delta t)_{t\to 0} \quad (1)$$

Where C is specific heat capacity calculated as a mass of magnetic carriers per equivalent of medium and it describes the “rate of temperature rise”, expressed as average absorbed power per mass unit (W/g). ΔT/Δt is the temperature increase per unit time or initial slope of the temperature versus time dependence. The SAR or SLP of a sample can be estimated experimentally by calorimetric methods.

SLP is defined as electromagnetic power lost per magnetic material mass unit and is expressed in watts per kilogram (W/kg) [36]. In the context of magnetic hyperthermia, the SAR and SLP are of the same order of magnitude. SLP was coined much later because SAR is somewhat misleading by two main reasons: i) it was used in the context of high-frequency radiation (microwaves or higher) where the formula and mechanisms for energy absorption by human tissues are different from the low-frequency magnetic mechanisms observed in magnetic hyperthermia; and ii) because "Absorption Rate" does not state what is being absorbed. SLP is more accurate since it is mass-normalized (specific) and denotes the magnitude (power) that is being absorbed/released. Since most of the data collected are in terms of SAR values, we will consider SAR values throughout the literature unless specified otherwise.

Since SLP or SAR should be as large as possible in the case of hyperthermia application, it can be expressed as being proportional to the rate of the temperature increase (ΔT/Δt). From the linear response theory (LRT) using homogeneity approximation, all spins in a nanosystem behave in the same linear way in response to the applied ac field. LRT indicates that while

decreasing size (increasing surface/volume ratio), more spins in the nanoparticle respond to the ac magnetic field in the same way [37]. This model predicts that the highest heat efficiency valid for 15-20 nm particles (ignoring the realistic conditions in *in-vivo* or *in-vitro* experiments). It is noted that besides the high SLP values, for *in-vivo* experiments, it is necessary also to consider biological constraints (Atkinsons's criterions) such as highest possible SLP within the biological limit, known now as "Brezovich criterion" (product of field amplitude (H) and frequency (f) maximum heat dose < 4.85 x $10^8$ $Am^{-1}s^{-1}$) and improvisation of "nano" objects in terms of heating efficiency [37].

$$SLP = \frac{C}{m}\left(\frac{dT}{dt}\right)_{t\to 0} \qquad (2)$$

where m is the mass of heat generating material, C the thermal capacity of the sample as a whole and (dT/dt) the rate of temperature increases as a function of time. Using the initial slope (dT/dt) in *T versus t (t →0)* curve, it provides a more real estimate of the SLP because the initial thermal losses (during heating process) are still negligible and the temperature distribution within the sample is more homogeneous.

Since SAR describes the efficiency of heat conversion, it is an important parameter from which one can determine the dosages applied to a tumor to achieve a reliable inactivation of target cells. For materials with high SAR, it is possible to reduce the dose applied to the patient to a minimum level. For MNPs, size, shape and microstructure can influence the value of SAR [38], NPs with high surface anisotropy can generate higher SAR value than that in the bulk form.

The dependence of SAR value to the structural parameters of the NPs and their surface modification makes it virtually impossible to compare the results from different research groups [12]. A comparable calculation of SAR value requires an expensive adiabatic set-up and

there is no clear agreement in which frequency or field amplitude used in the experiments can be compared. To overcome this issue, a term intrinsic loss power (ILP) has been introduced by Pankhurst *et al.* [39] in which SAR is being normalized by the frequency and field amplitude, and therefore independent of the magnetic field parameters. For ILP, it allows a more direct comparison of the heating efficiency of superparamagnetic NPs. The ILP parameter, however, is not completely intrinsic and the system has to follow a few assumptions: the size of the crystallite needs to have a polydispersity index greater than 0.1; the frequency used in the experiment of several MHz; the H value of the sample much greater than the saturation of the NPs and the thermal losses of the system have to be reproducible [32]. Following these assumptions, ILP can be defined as:

$$ILP = SAR/H^2 f \qquad (3)$$

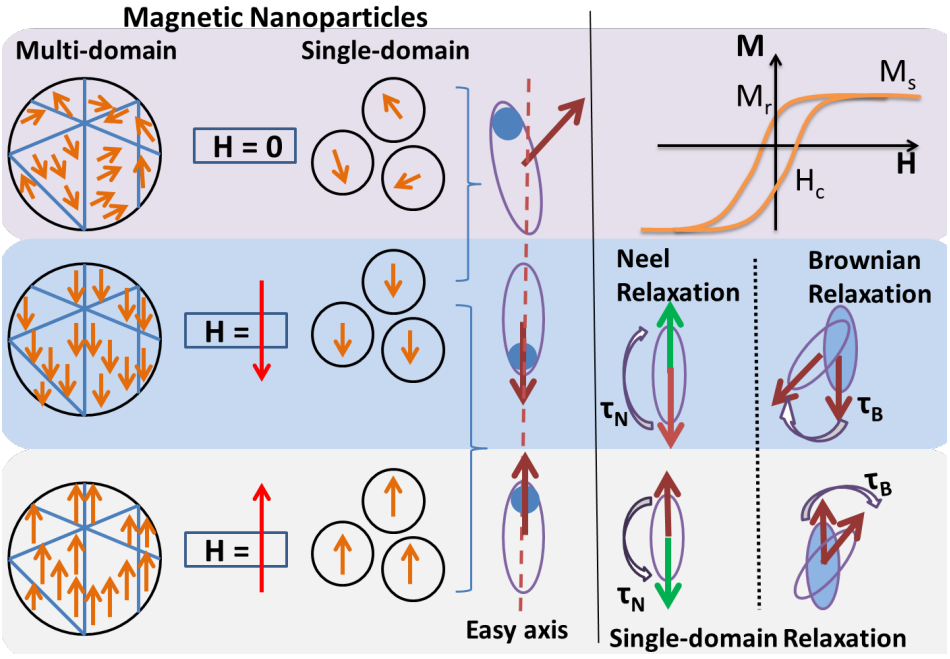


**Fig. 2:** Different heat generation models in a MNPs in response to the ac magnetic field (H).

### 2.1. Mechanisms of magnetic-induced hyperthermia

The heating properties of the MNPs are due to hysteresis, Néel and Brown mechanisms. Different heat generation models in a MNPs in response to the ac magnetic field are shown in Fig. 2.

#### 2.1.1. Hysteresis mechanism

Hysteresis mechanism of magnetic hyperthermia commonly referred as hysteresis loss is due to multidomain NPs (Fig. 2). The magnetic structure of ferromagnetic materials spontaneously splits into domains in which each of them has uniform magnetization of all the magnetic spins aligning in one direction. The domains are separated by domain walls. When the material is subjected to a cycle of magnetic fields, the magnetization shows a non-linear curve called a hysteresis loop which is a measure of energy dissipated per cycle of magnetization reversal (Fig. 2). This loop is characterized by three material dependent parameters: saturation magnetization $M_s$, remnant magnetization or remanence $M_R$ and coercivity $H_c$ [34]. During a cycle of magnetic fields, there are two processes contributing to hysteresis losses namely the displacement of domain walls being pinned and released at inhomogeneities and the rotation process of magnetic moments inside domains [38].

For low field amplitudes, losses per cycle depend on the field according to a third order power law, commonly denoted as the Rayleigh law, which is theoretically explained by wall pinning. With decreasing particle size, a transition to single domain particles occurs in which the process of magnetization reversal is in the simple uniform mode. Single domain particles with uniaxial anisotropy were theoretically treated in the classical paper of Stoner and Wohlfarth showing

the highest amount of hysteresis energy. The equilibrium magnetization direction is determined by anisotropy contributions due to crystal structure, particle shape and surface [40].

If an assembly of MNPs is put into an ac magnetic field of frequency *f* and amplitude $\mu_0 H_{max}$, the amount of heat 'A' released by the MNPs during one cycle of the magnetic field remains equal to the area of their hysteresis loop. The amount of heat released by ferromagnetic material through hysteresis loss is given by

$$A = \int_{-H_{max}}^{+H_{max}} \mu_0 M(H) dH \quad (4)$$

then, $$SAR = Af \quad (5)$$

where *f* denotes the frequency of the ac magnetic field expressed as $f = \omega/2\pi$, M magnetization and H applied ac magnetic field. Area of the hysteresis loop depends upon the various factors such as MNPs size, anisotropy, frequency and amplitude of applied ac magnetic field etc. Here, $H_c$ and $M_R$ are reduced for larger particles due to the reduction in the energy loss per cycle. For smaller particles the enhanced anisotropy energy barriers separating the different orientation states gives enhanced energy loss causing the blockage of the magnetization in the case of superparamagnetic NPs [41].

### 2.1.2. Néel mechanism

For single domain MNPs, the energy barrier for magnetization reversal decrease and consequently thermal fluctuations lead to relaxation phenomena which is commonly called Néel mechanism or Néel relaxation (Fig. 2) [34]. In this case, the time constant of the ac magnetic field is short enough that the physical orientation of the particle remains unchanged while the moment alternates between parallel and antiparallel orientations. These oscillations

in the magnetization can occur in a specific time, called the relaxation time ($\tau_N$). The characteristic time related to the thermal fluctuation of magnetization with different anisotropy axis is given by Néel-Arrhenius equation:

$$\tau_N = \tau_0 e^{\frac{KV}{k_B T}} \quad (6)$$

where $\tau_0$ is the characteristic flipping frequency of about $10^{-9}$ s, K the anisotropy constant, V the volume of the magnetic particle, $k_B$ the Boltzmann constant and T the temperature. Hence, Néel mechanism depends exponentially on magnetic anisotropy and particle volume. The relationship between anisotropic constant K and thermal energy $k_BT$ provides the relaxation of the inner magnetic core. Néel relaxation prevails when there is higher frequency as well as smaller particle size [42].

**2.1.3. Brownian mechanism**

In fluid containing magnetic particle suspension, a relaxation path which occurs due to the ability of particles to rotate freely is termed Brownian relaxation. In this case, heating of the particles in liquid suspension occurs due to viscous drag between the particles and the liquid, where the entire particle has a rotational movement with an applied ac magnetic field, while the magnetic moment remains fixed relative to the crystal axis (Fig. 2). The Brownian relaxation time ($\tau_B$) is given by the following equation [43]:

$$\tau_B = \frac{3\eta V_H}{k_B T} \quad (7)$$

Where η is the viscosity of the liquid carrier, $V_H$ the hydrodynamic volume of the particle, $k_B$ the Boltzmann constant and T the temperature. Generally, the hydrodynamic volume $V_H$ is larger than the volume of the particle due to fluid interactions or absorbed surfactant. The particles

can physically rotate depending on the hydrodynamic parameters of both the particles and the medium at a characteristic time [41]. The Brownian relaxation is size-dependent being dominant at the higher particle size and strongly viscosity dependent. Brownian losses are not only found in superparamagnetic NPs but can also be observed for other if the viscosity of the surrounding medium is low enough to allow rotation of the complete particle.

Generally, both Néel and Brownian relaxations can occur in parallel and the effective relaxation time, $\tau_{eff}$, can be determined by the following expression:

$$\frac{1}{\tau_{eff}} = \frac{1}{\tau_N} + \frac{1}{\tau_B} \quad (8)$$

which is dominated by the shorter Néel and Brownian relaxations. For *in vivo* and *in vitro uses,* it is better if MNPs relax essentially through the Néel mechanism because of the change in the viscosity medium around the cells limiting free rotation of the particles [12, 44]. In accordance with the LRT theory, the loss power density P is expressed as [45]:

$$P(f, H) = \mu_0 \pi \chi''(f) H^2 f \quad (9)$$

Where $f$ and H are the frequency and magnitude of an applied magnetic field, respectively, $\mu_0$ the permeability of free space, and $\chi''$ the imaginary part of the susceptibility.

**2.2. Parameters affecting magnetic-induced hyperthermia**

**2.2.1. Effect of applied magnetic field and frequency**

The heat dissipation value is proportional to the applied ac magnetic field strength and frequency. For magnetic induced hyperthermia, the amplitude is proportional to the square of the applied ac magnetic field amplitude as shown in eq. 9. SAR is generally found to increases with increasing field strength. In clinical application, the strength of magnetic field is limited by

physiological considerations and that with large amplitude, high frequency may induce local heating in non-magnetic tissues due to induced eddy currents [45]. Here the optimum choice of field amplitude may differ for different samples even with the same maximum SAR values.

The role of magnetic field frequency in SAR is considerably more complex in which its range depends on the degree of magnetic anisotropy (K) of MNPs [45]. The frequency of the ac magnetic field must be enough to provoke the targeted intra-tissue hyperthermic heating phenomenon but not too high to cause overheating of healthy tissues. It was reported that the frequency should be in the range of 100–1000 kHz in order to prevent side effects of the ac magnetic field *in vivo* [46]. Using the kinetic Monte-Carlo model with its accurate timescale quantification, it is possible to have a reliable prediction of the frequency and particle size dependent behavior.

For a safe application of hyperthermia to patients, the recommended product of the frequency and the magnetic field amplitude C should be smaller than $5\times10^{9}\ Am^{-1}s^{-1}$ but in many experiments it was found mostly above this limit [47, 48]. By introducing the condition $f(H) = C/H$ into the dependence $SAR(f,H)$ for the different loss processes discussed above one get the optimum combination of $f$ and $H$ for maximum SAR. The combination of ac field amplitude and frequency for magnetic hyperthermia depends strongly on the type of particles provided for therapy.

### 2.2.2. Effect of particle size

The optimum particle size showing enhanced heating efficiency for magnetic hyperthermia is still a matter of debate mainly due to the lack of conclusive data to date comparing the predicted and *in vivo* performance of MNPs for a wide range of tumors. However, the role of

size and size distribution on the heating properties of particles will be significant and of relevant interest. Heat dissipation mechanism is expected to depend largely on particle size but there are two complicating factors that make its contribution to a specific heating mechanism difficult: i) the particles may have single or multiple crystal domains, and ii) the size distribution of NPs can be widely dispersed for a given sample. For magnetite NPs synthesized in the range of 8-18 nm, the largest particles displayed the highest SAR values [49]. The effects of size distribution on heating rate in magnetic fluids was theoretically addressed by Rosensweig *et al.* [50] highlighting the importance of using monodisperse colloids in heating experiments. A narrow size distribution needs a good adjustment of mean particle size in relation to the magnetic field amplitude for attaining maximum SAR.

The three primary mechanisms (hysteresis loss, Brownian relaxation and Néel relaxation) of heat generation in magnetic induced hyperthermia depend largely on the size of the particle. Hysteresis losses dominate in large particles (> 100 nm), and particles of this size are too large for many clinical applications. For magnetite below 25 nm, particles become superparamagnetic with negligible hysteresis losses leaving Néel and Brownian relaxation the main relevant mechanisms [51]. Generally, within this range, Brownian relaxation is significant in larger particles and Néel relaxation in smaller ones; however, exactly where this division occurs depends strongly on the anisotropy constant of the particle [49, 52].

It was reported that the iron oxide NPs (IONPs) with narrow size distribution and with a mean diameter that corresponds to the maximum coercivity in the single domain size range could lead to maximum heating efficiency [53]. In the superparamagnetic regime SAR increases with increasing relaxation time (*i.e.* with increasing particle size) until the validity of the relaxation

theory ceases near the transition to the stable single domain regime. The particle systems with narrow size distribution are capable of providing remarkable output of heating power and superparamagnetic samples increase SAR with increasing particle size [47].

Harabech *et al.* [54] demonstrated the influence of relaxation time constant $\tau_0$ on SAR using a macrospin model. Here, the Landau-Lifshitz-Gilbert equation was used to investigate the relation between the Gilbert damping parameter and $\tau_0$. It was found that although the effect itself can be quite large, size dependence of $\tau_0$ is not vital in SAR calculations because in each size distribution only a limited size range of MNPs contribute to the heat generation. In the investigated model, a well-chosen $\tau_0$ was used. The precise value of $\tau_0$ is most accurate when it is as close as possible to its true value for the radius of magnetic NPs at the peak of the heating [54].

**2.2.3. Effect of particle Morphology**

Surface properties are crucial for NPs' characteristics and its modification will lead to the changes in their physical, chemical and biological properties [55]. Several investigations regarding surface and shape morphologies were reported to understand the magnetic characteristics and their magneto-hyperthermia effect [56]. The studies include new designs or morphologies, for example core–shell, onion-type, multilayered, alloys, multi-metallic etc. Core-shell NPs are class of hybrid materials, where composition and microstructure varies in the radial direction and it can provide the multi-functionalities. The core-shell NPs offer a number of advantages over mono metallic/metal oxide NPs for hyperthermia-based therapy including: (i) a shell can protect air sensitive high magnetic moment nanocomponent core, which provides high value of SLP [57]; (ii) reduction in the anisotropic magnetic dipolar interaction in core-shell

NPs helps to increase the stable suspension of magnetic fluids (behaves as isotropic dispersions) even in the absence of an external magnetic field, which is the main problem in mono/single metallic magnetic NP *e.g.*, maghemite@$SiO_2$ NPs [58, 59], and (iii) it offers enhanced hyperthermia response [60].

Hemery *et al.* [61] prepared well-defined multi-core assemblies of nanoflowers with narrow grain size dispersity and studied magneto-caloric effect in detail along with applications for MRI agents depending upon the morphologies and cluster sizes. They found the correlation between SAR at given field amplitude ($H_{app}$ = 10.2 kA/m) and frequency (f = 755 kHz) against outer diameter measured by TEM, experimentally following a quadratic law for nanospheres, and a lower exponent (nearly square-root) for nanoflowers, in agreement with the models on the optimal size of MNPs for magnetic hyperthermia at given values of specific magnetization and magnetic anisotropy. The study indicates that nanoflowers and the largest spheres find applications as magnetic nano-heaters, while smaller NPs do not generate sufficient heat [62].

Recently, Sol-Fernandez *et al.* demonstrated a wide range of studies regarding intracellular hyperthermia under exposure of alternating magnetic field on flower like Mn-doped iron-oxide functionalized with $\alpha_v\beta_3$-integrin-ligand [63]. They were able to demonstrate intracellular heating capacity of MNPs depends on factors such as cytoplasm viscosity, NP aggregation within subcellular compartments, and dipolar interactions. Three major strategies were adopted to maximize the magnetic hyperthermia efficiencies [63]: (i) varying doping of $Mn^{2+}$ changes the crystalline anisotropy in inverse cubic structure; (ii) changes in shape of NPs but keeping superparamagnetic characteristics; and (iii) increasing cell-particle efficacy and

interactions through conjugation with a biological targeting molecule to reach the nanoparticle concentration required to increase the temperature within the cell.

### 2.2.4. The role of anisotropy on heating efficiency

Anisotropy of MNPs is a crucial parameter for tuning the magnetic hyperthermia and, according to LRT, it is important in enhancing the Néel relaxation [64, 65]. The most common types of anisotropy are magneto-crystalline anisotropy (or magnetic anisotropy or crystalline anisotropy), surface anisotropy, shape anisotropy, exchange anisotropy and induced anisotropy *(e.g.* by stress). In MNPs, shape anisotropy and magneto-crystalline anisotropy are the most important. Magneto-crystalline anisotropy arises from spin-orbit interaction which depends on the type of material, temperature and impurities. With decreasing the size of NPs, the ratio of the number of surface atoms to that of the bulk become larger yielding larger contribution of the surface magnetization. In this case, the surface anisotropy of MNPs could be more significant than both the magneto-crystalline and shape anisotropy [53].

The heating efficiency of spherical IONPs has been widely studied. Different shapes of IONPs other than the typical spheres, *i.e.* cubes, octopods, octahedral, cube-octahedral and disc shapes, have been proposed in order to tune their anisotropy and improve the heating efficiency [66, 67]. In experimental studies, the comparison of (Zn doped)cubic and (undoped)spherical IONPs with similar magnetic volumes showed more than two-fold increase in SAR for the cubic one [68]. Single-domain cubic IONPs are reported to possess superior heat induction power compared to spherical ones of similar size due to the higher surface magnetic anisotropy and the tendency towards aggregation into chains facilitated by the cubic shape [69]. In addition, monodisperse $Fe_3O_4$ nano-octopods were reported to show better heating

efficiency than their spherical counterparts, especially in the high field region (> 400 Oe) [70]. The $Fe_3O_4$ nanorods have shown enhanced SAR values (862 W/g for an ac field of (68 kA/m) relative to their spherical and cubic counterparts of similar volume (~140 W/g and ~314 W/g, respectively), owing to their higher saturation magnetization and effective anisotropy. The SAR of $Fe_3O_4$ nanorods can be tuned by varying their aspect ratio [69]. $CoFe_2O_4$ based magnetic fluid was found to have lower SAR than $Fe_3O_4$ and $MnFe_2O_4$ based magnetic fluids. Even after optimizing particle size of $CoFe_2O_4$ system, higher SAR values could not be achieved because of its high anisotropy energy [71].

**2.2.5. Effect of Dipolar interaction**

Understanding the role of dipolar interactions in magnetic hyperthermia experiments is important for optimization of NPs heating power and for selecting the correct dose to inject to reach the desired outcome in intracellular magnetic hyperthermia therapy. For *in vivo* applications, uptake of MNPs in sub-cellular vesicles such as lysosomes can lead to aggregation resulting to the change of magnetic hyperthermia properties due to dipolar interactions [72]. The investigation of dipolar interaction carried out via numerical simulations based on a mean-field model showed that it can be used to increase the dissipation of magnetically soft particles but should be avoided in the case of hard particles. It may connect to the fact that the dipolar interaction acts to increase the effective anisotropy barrier. Magnetically hard particles were seen to be further hampered by increasing the dipolar interaction due to a larger freezing of the magnetic spins [73]. Using Monte Carlo algorithm, hysteresis area was found to be well correlated with the parallel or antiparallel nature of the dipolar field acting on each particle.

The magnetic interactions strongly depend on NP diameter and anisotropy as well as on the amplitude of the applied magnetic field [74, 75].

It is also reported that a shortening of the magnetization (Neel) relaxation time when increasing the dipolar interactions. Here, dipolar effects occur as soon as the inter-particle distances become shorter than about three times the particle diameter [76]. As the inter-particle distance decreases, it increases dipolar interactions which alter the magnetic response of the ferrofluid. This interaction directly affects the Néel relaxation time which is the dominant mechanism in hyperthermia studies of the small NPs (< 10 nm) [52]. Further, since dipolar interactions are related with anisotropies directly [77], tuning the magnetic anisotropy without affecting significantly the size/ size distribution of NPs, affects the efficiencies of nano-heaters at low field hyperthermia, which is the first requirement of clinically relevant criteria. Lowering anisotropy decreases the fraction of blocked NPs, hence increasing the number of nano-heaters (*e.g.* Zn doped Mn-ferrite will have higher SLP at low field hyperthermia in comparison to Co doped Mn-ferrites, even if the particle size distributions are similar [78–80]). Although for single magnetic particle, bigger size can result in enhanced hyperthermia, in the assembly of MNPs the increase in size can give rise to the large dipolar interaction and its dominating effect can reduce the overall magnetic hyperthermia effect.

Experimental evidences and Monte Carlo simulations of an assembly of monodisperse single domain MNPs in thermal equilibrium have shown that the dipolar interactions significantly affect the magnetic susceptibility and hysteresis losses resulting in a considerable reduction in specific heating power for hyperthermia applications [81].The heating efficiency of a magnetic colloid can increase or decrease with dipolar interactions or the colloid concentration. The

power dissipated by an ensemble of dispersed MNPs becomes negligible as a direct consequence of the long-range nature of dipolar interactions [82]. The huge enhancement of a heating temperature of soft $MFe_2O_4$ (M = Mg, Ni) from 17.6 to 94.7 °C and from 13.1 to 103.1 °C ($NiFe_2O_4$) NPs was found due to the increase in magnetic hysteresis and relaxation losses associated with the increase in magnetic moment and susceptibility induced by the dipole interaction [83].

**2.2.6. Effect of Viscosity**

Unlike Néel relaxation, the heat dissipated through Brownian relaxation is greatly influenced by the viscosity of the medium that tends to counter the movement of particles in the medium [56]. For example, if the viscosity of the medium is high or if the freedom of particle rotation is suppressed, the heat dissipated will either diminish or seized [44, 84]. As the temperature increases the heating rate in magnetite-maghemite NPs studied for three different particle sizes (5, 28 and 45 nm) increases due to the decreasing viscosity of the medium [85]. The viscosity has a deleterious effect on magnetic heating. The SAR values for fluid of magnetite coated with dextran (MAG D) NPs and maghemite nano-powders decreased when the NPs were dispersed in more viscous environments due to a reduction in the Brownian relaxation component of magnetic heating [49]. From another similar experimental study, it was concluded that the heating ability of NPs was reduced with an increasement in viscosity. Thus, it was anticipated that due to the high viscosity of the extracellular matrix in a biological tissue, the heat loss by Brownian relaxation is negligible [86].

**2.2.7. Effect of coating with organic ligands**

The molecules chosen for stabilizing the NPs also determine the *magneto-hyperthermia of* the NPs once exposed to the biological media, because of the formation of a protein corona that influence the particles' behavior [87]. *In-vivo* and *in-vitro* MH experiments suggest that magnetic NPs coated with different organic ligands (polyethyleneimine (PEI), polyethylene glycol (PEG), dextran, oleic acid, and Pluronic F-127) behave differently as compared to uncoated magnetic NPs [63]. An efficient stabilization increases the biocompatibility of NPs, limiting the immune response and avoiding the formation of protein NPs aggregates which can reduce the chance of obstructing blood capillaries [88]. The introduction of organic ligands on the surface of NPs improves the uptakes to tumors and cells by increasing the time the NPs spent in the bloodstream and reducing toxicity. Organic ligands do not affect directly much heat dissipation of magnetic NPs, but they affect their hydrodynamic sizes and dispersion, hence their Brownian relaxation ($\tau_B$). Linh *et al* have shown that the SLP of dextran coated $Fe_3O_4$ NPs was more than 2 times efficient compared to the uncoated $Fe_3O_4$ ones [61]. The influence of stabilizing ligand on biocompatibility and cellular uptake *in vitro* was studied by Pradhan *et al.* using different coatings of dextran and lauric acid on $Fe_3O_4$ NPs [71]. It was observed that lauric acid-coated $Fe_3O_4$ NPs were less biocompatible and had a higher uptake than that of dextran-coated ones, when tested on L929 mouse fibroblast cells which could be attributed to different cellular interactions from the coating materials [62]. Here, the choice of a biocompatible capping agent could increase the uptake of the NPs in the tumor, the time spent in the blood stream by the particles, the heating efficiency and reducing the aggregation of the particles *in vivo*.

**2.3. Potential magnetic-induced hyperthermia nanomaterials**

MNPs can also be designed to combine several therapeutic functions like therapy and drug delivery as well as therapeutic and diagnostic functions. At the same time, MNPs must have characteristics to qualify for biomedical applications such as biocompatibility, nontoxicity, ability to escape from the reticuloendothelial system and low protein absorption. The number of various types of possible core NPs ranging from metallic Fe, Co, Ni, Gd, and their oxides to Au, Ag, carbon nanotubes, manganese oxide, micelles, liposomes etc. Iron oxide based NPs have been extensively investigated due to their excellent superparamagnetic, biocompatible, and biodegradable properties [20, 56]. There have been extensive studies recently on tailoring and tuning the properties of the NPs by changing the structure, composition, size, and shape via different syntheses. Reviews on synthesis of nanomaterials will not be our focus and can be found elsewhere [89–92]. For MNPs, the effective hyperthermia heating agents are of paramount importance which would enable selective heating of tumor cells and vasculature avoiding excessive damage to healthy tissue structures.

**2.3.1. Iron oxide nanoparticles (IONPs)**

Among magnetic materials, IONPs are considered to be one of the best candidates for biomedical applications due to their biocompatibility, accessibility, facile synthesis [93], chemically stability and superparamagnetism. IONPs of either magnetite ($Fe_3O_4$) or maghemite ($\gamma$-$Fe_2O_3$) are the most widely use and they have been proved to be well tolerated by the human body which have been approved by the US Food and Drug Administration (FDA) [93]. Superparamagnetic IONPs (SPIONs) have multifunctional characteristics including image-based diagnostics, localized destruction of target cells via magnetically induced heating and drug release for use as a multimodal cancer therapy agent [93–95]. These properties make SPIONs

an excellent candidate for magnetic hyperthermia therapy since heat generation can be controlled/modulated by an externally applied ac magnetic field. In dual magneto-photothermal therapeutic approach with only IONPs as heat mediators, a very efficient heat conversion for both modalities was achieved. Remarkably, the dual magneto-photothermal therapeutic approaches of IONPs resulted in complete cell death *in vitro* and in total solid tumor ablation *in vivo* at low iron doses, tolerable magnetic field and frequency conditions as well as acceptable laser power doses [14].

Theoretical analysis has shown that the heating efficiency of IONPs depends on their properties such as the saturation magnetization, anisotropy energy and rate of magnetic relaxation. In this regard, size is a controlling factor for increasing the heating efficiency. IONPs with sizes > 20 nm have a SAR significantly higher than that predicted by the widely used linear theory of magnetic fluid heating [94]. The narrowest size distributions, however, have been found in magnetite crystals in bacterial magnetosomes, which have been shown to be significantly more efficient than chemically precipitated particles of similar size [52]. In MNPs comprising iron oxide cores with mean diameter of 50 nm surrounded by a dextran layer, saturation magnetization of the shell is found to play a crucial role in determining SAR [96].

**2.3.2.Ferrites for magnetic hyperthermia**

For clinical conditions to cure cancer, hyperthermia is a key technique, but temperature regulation is very important that must be precisely controlled. In general, a higher coercivity is required to generate more energy during one cycle of heating which can be achieved using metal NPs. Zhang *et al.* studied optimization of Curie temperature and coercivity of Co-Zn ferrite NPs aiming for the custom design of self-regulating hyperthermia nano-vehicles by

substituting a pre-determined quantity of $Cr^{3+}$ through a hydrothermal process [97]. In $Zn_{0.54}Co_{0.46}Cr_{0.6}Fe_{1.4}O_4$ NPs the Curie temperature is 45.7 $^{o}$C and coercivity $H_c$ = 174 Oe. The temperature of these NPs suspension can be self-regulated at 44.0 $^{o}$C, close to but critically under the clinically used magnetic fields. The evaluation of *in vitro* cytotoxicity of $Zn_{0.54}Co_{0.46}Cr_{0.6}Fe_{1.4}O_4$ NPs also suggested low toxicity and so the NPs could potentially be used in cancer therapeutics for precise energy transfer from the external magnetic field to the tumor via a self-regulating delivery system in hyperthermia [97]. In summary, the data obtained show the bespoke synthesis of NPs to provide the necessary physical platform to regulate not only the Curie temperature but also the coercivity by a change in the microstructure.

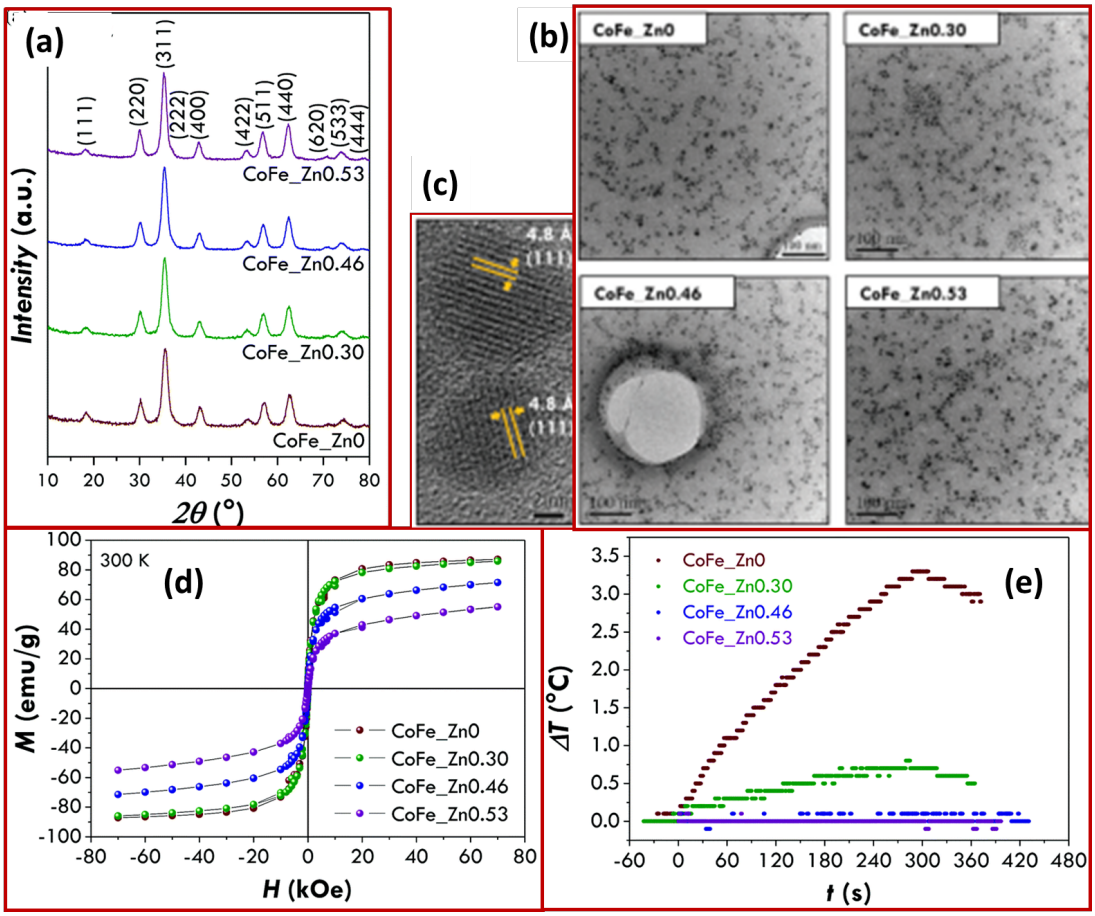


**Fig. 3**: Microstructural and morphological properties of CoFe_$Zn_x$ (with x = 0, 0.30, 0.46, 0.53) samples: (a) XRD patterns obtained by the Cu Kα source-equipped diffractometer, (b) TEM

images obtained by the JEM 2010 UHR, (c) high resolution images, (d) Magnetisation versus magnetic field curves of CoFe_$Zn_x$ samples measured at 300 K. (e) Heating curves of CoFe_$Zn_x$ samples at 25 °C, obtained under a magnetic field of 183 kHz and 17 kA/m [98]. (Reprinted with permission from Ref. [98]. Copyright 2016, The Royal Society of Chemistry)

Similarly, Mamely *et al.* [98] discussed about Zn-substituted cobalt ferrite NPs ($Zn_xCo_{1-x}Fe_2O_4$ with $0 < x < 0.6$) as shown in Fig. 3, having similar particle sizes (~7 nm), size distributions and capping agent amount of 15 %. Here, $CoFe_2O_4$ has shown a triple SAR value of 19 W/g and it has both the Néel and Brownian relaxation times that match the characteristic time of the hyperthermic measurement. On the other hand, $Zn_{0.3}Co_{0.7}Fe_2O_4$ has a faster effective relaxation time in light with the linear response theory that suggests the higher efficiency of the $CoFe_2O_4$ sample.

**2.3.3. Multifunctional hybrid systems**

Multifunctional hybrid NPs being comprised of two or more distinctive functional components have garnered considerable attention in recent times over mono-functional ones. In "all in one probe" mediated by hybrid MNPs, Au/MNPs assimilated into poly(lactic-co-glycolic acid)(PLGA) NPs which can target cancer cells. Au/MNPs can deliver therapeutic cargos to the cancer cells and exert its lethality by three distinctive modes (*i.e.* chemotherapeutic, photothermal and magnetic hyperthermia) either independently or by the synergistic action of drug and hyperthermia [99].

Ferrite based hybrid composites have received special attention due to various biomedical applications. A promising nanocomposite material, which was composed of $MnFe_2O_4$ NPs of ~17 nm in diameter deposited onto graphene oxide nanosheet synthesized using a modified co-precipitation method, showed enhanced high-field SAR due to the increase of effective

anisotropy and the reduced aggregation of the $MnFe_2O_4$ NPs on the graphene oxide [100]. The exchange coupling between a magnetically hard core and magnetically soft shell can tune the magnetic properties and maximize the specific loss power.

A multifunctional nanocomposite consisting of graphene oxide–iron oxide -doxorubicin (GO-IO-DOX) provides multiple therapeutic functions in addition to imaging capabilities. *In vitro* studies revealed that the GO-IO-DOX nanocomposites possess a greater therapeutic efficacy by exhibiting a superior hyperthermic response in an ac magnetic field and cancer cell specific DOX release to effectively exterminate the target cancer cells through apoptosis-mediated cell death [101].

**2.3.4. High magnetic moment core@shell nanoparticles**

Recently, core@shell MNPs have emerged as an effective class of NPs to optimize magnetic loss heating. Here, a shell can act as a protective shield for sensitive core material. Anisotropy constant (K) provide an extra degree of freedom to tailor nanoscale magnetism of core@shell. Core@shell MNPs with various shapes such as cubes, octapods, octahedrons, cuboctahedrons, dimers, triangles and flowers have been studied to understand the effects of the core–shell interface structure on the exchange coupling interaction and the resulting heating efficiency [102]. The surface of the uniform core@shell nanocomposite could be further functionalized with new ligands to give well-defined structure.

Core@shell $Fe@Fe_xO_y$ NPs have the potential to be promising tools for many applications [103], thanks to their combination of an iron core, with a high magnetic moment and an iron oxide shell which could protect the core from oxidation (Fig. 4). However, the deterioration of NPs structure can lead to the shrinking of the core and the hollowing of the structure, diminishing

the magnetic properties. The ability to retain the iron core under biomedically compatible conditions is desirable for many applications.

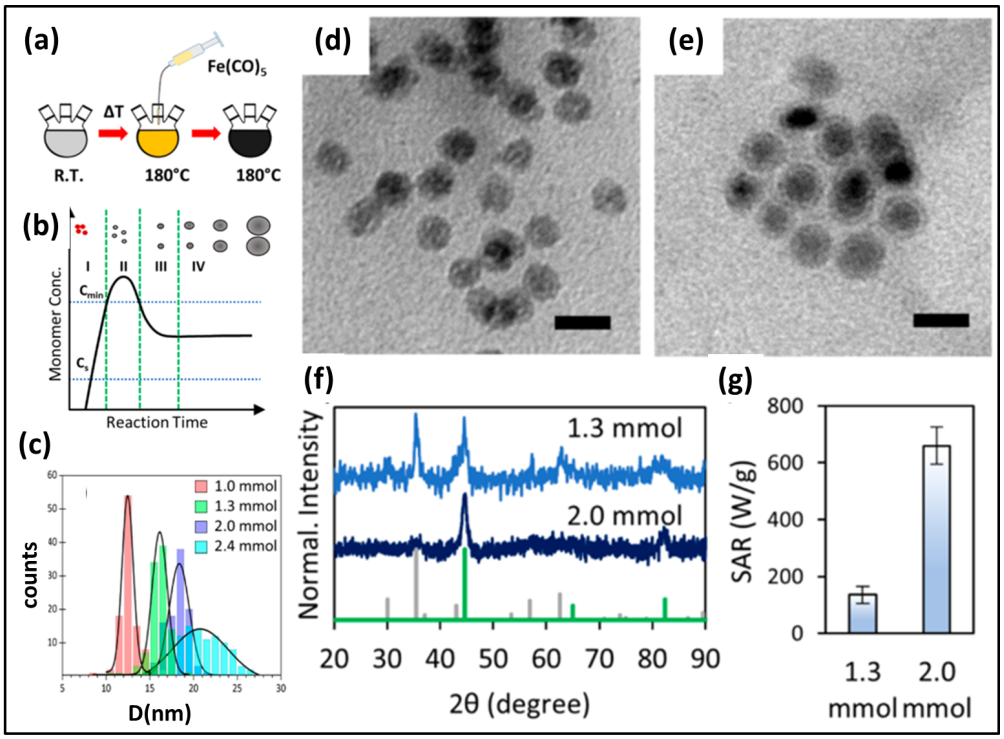


**Fig. 4** (a) Schematic illustration of the synthesis. (b) Extended LaMer plot configuration, (c) Size distribution for the four reactions with different amount of precursor $Fe(CO)_5$ used: 1.0, 1.3, 2.0 and 2.4 mmol. TEM (with 20 nm of scale bar) picture of Fe NPs synthesized with (d) 1.3 and (e) 2.0 mmol of $Fe(CO)_5$ (f) XRD patterns shown with the gray reference pattern corresponding to the $Fe_3O_4$phase and the green one to the Fe phase. (g) Heating power for the two systems measured at 303 kHz and 24 kA/m. Error bars indicate the standard error of the means of different SAR measurements [103]. (Reprinted with permission from Ref. [103], Copyright 2018, American Chemical Society).

In this work, Farmiani *et al.* [103] have developed a synthetic method to produce core@shell α-$Fe@Fe_xO_y$ NPs with tuneable sizes and evaluated the retention of the stable magnetic α-Fe core upon exposure to air and after ligand exchange and its resulting effect on the magnetic hyperthermia. Using a continuous injection of the precursor, we were able to finely tune the

final size of the core@shell NPs producing four samples with average sizes of 12, 15, 18, and 20 nm. The structural properties of the particles were studied, and while the size increases, the chemical stability of the iron core is enhanced, and the magnetic properties improved accordingly. Particles larger than 20 nm were shown to be prone to aggregation, resulting in an abrupt increase of the particle size distribution. Two samples (Figs. 4d&e) with high magnetization saturation value and low polydispersity, 15 and 18 nm, were transferred in water using a dopamine-functionalized poly(isobutylene-alt-maleic anhydride) polymer, resulting in colloidal stability over a wide range of pH and ionic strength comparable to physiological conditions. We found that the 18 nm particles retain their chemical properties over 2 months, with less oxidation of the Fe core; this results in a specific absorption rate (SAR) value of 660 W/g and intrinsic loss power (ILP) of 3.6 $nHm^2\ kg^{-1}$ (Fig. 4g) , while the 15 nm NPs resulted in the reduction of their properties due to oxidation of the core.

Au–$Fe_xO_y$ hybrid structures offer two different functional peripheral surfaces, rendering them particularly attractive multifunctional probes for specific applications. The heat generated by $Fe_3O_4$@Au core@shell nanocomposites is higher than that of $Fe_3O_4$ NPs in the same condition in which it should be related to the higher magnetic anisotropy of the superparamagnetic fraction with the Au shell and higher heat capacity of the Au shell [104].

In a core@shell MNPs combining a soft Mn ferrite and a hard Co ferrite, a theoretical framework was developed to include the crystal anisotropy contribution of the Co ferrite phase to the total anisotropy. The experimental results confirmed the theoretical results of the hysteretic heating loss when including nonlinear effects in an effective susceptibility. It is the

relative fraction of Co ferrite which determines the anisotropy of these exchange-coupled core@shell independently of the NP size [105].

The optimization of anisotropy constant (K) and saturation magnetization ($M_s$) by varying the composition of core@shell MNPs give enhanced SAR. By varying the combination of $CoFe_2O_4$-based core@shell MNPs, *i.e.* $CoFe_2O_4$@$MnFe_2O_4$, $CoFe_2O_4$@$Fe_3O_4$, $MnFe_2O_4$@$CoFe_2O_4$, $Fe_3O_4$@$CoFe_2O_4$, $Zn_{0.4}Co_{0.6}Fe_2O_4$@$Zn_{0.4}Mn_{0.6}Fe_2O_4$, SLP values range from 100 to 450 W/g for single-component MNPs and for core@shell NPs from 1,000 to 4,000 W/g [106]. The optimized core@shell MNPs have SPL values an order of magnitude larger than conventional IONPs and the therapeutic efficacy of these NPs is superior to that of a common anticancer drug.

Recently, He *et al.* [107] reported the maximized SLP and ILP approaching theoretical limits for ac magnetic-field heating of NPs. This was achieved by engineering the effective magnetic anisotropy barrier of NPs via alloying hard and soft ferrites. 22 nm $Co_{0.03}Mn_{0.28}Fe_{2.7}O_4/SiO_2$NPs reach a SLP value of 3,417 W/g at a field of 33 kA/m and f = 380 kHz. Biocompatible $Zn_{0.3}Fe_{2.7}O_4/SiO_2$NPs achieve SLP of 500 $W/g_{metal}$ and ILP of 26.8 $nHm^2/kg$ at field of 7 kA/m and f = 380 kHz below the clinical safety limit. This work guides for the design of NPs with appropriate magnetic properties for maximized heating power at any field parameters and, conversely given a particular NP type, choice of field parameters leading to maximized heating power. Furthermore, this biocompatible NP platform with greatly enhanced ac field heating at low field amplitudes are promising for targeted hyperthermia of small tumors and metastases.

**2.4. Instrumentation for magnetic-induced hyperthermia**

Although there have been several works reported on the magnetic hyperthermia from its parameter control (size, shape, distribution, etc.) to improve the heating capabilities of the NPs,

there are only few sophisticated systems in the market for measuring SLP. There are number of homemade systems for hyperthermia experiments to measure heat loss in the form of NPs fluid and also utilized for experimentation in mice. Here, the devices are usually built based on simple resonant RLC circuit to create ac magnetic field with a copper coil of different diameter, number of turns, cooling agents etc. In a study of contributions of Néel and Brownian relaxation mechanism to SLP, Fortin *et al.* [86] used a homemade device with a copper coil having diameter of 16 mm, frequency range of 300 kHz-1.1 MHz and amplitude up to 27 kA/m. The variation in frequency and amplitude has been made by using a variable capacitor (10 pF-4 nF) in series and self-inductance of 25 µH. To avoid heat generated by the coil, continuous circulation of nonane was maintained during the measurements. The small sample volume of 300 µL was used to ensure homogenous magnetic field and a fluoro-optic thermometer for temperature measurements. They presented the quantitative magnetic hyperthermia data matching with theoretical predictions considering relevant parameters such as size, materials, solvent and field characteristics. Ma *et al.* [108] used a 3 loops copper coil with frequency of 80 kHz and field amplitude of 32.5 kA/m for calorimetric measurements with an asbestos sleeve to reduce excessive heat produced by the copper coil. IONPs fluids were prepared in water with concentration of 2 g/L. Maximum value of SAR of 75.6 $W/g_{metal}$ was observed at particle size of 46 nm, where the heating contribution is dominated by hysteresis loss. Further increase in particle size showed low heat generation efficiency.

Sadat *et al.* [109] used a 10 turn coil of 84 mm long with an inner diameter of 39 mm. A sinusoidal 13.56 MHz frequency signal had been generated by a radio frequency generator. Cold water circulation was used to cool down the coil with high ac current and a fiber optic

sensor (FOT-L-SD) to measure the temperature. They observed high SAR values for uncoated NPs as compared to coated or confine NP in another material such as iron oxide in Si shell. The observed results were attributed to the high absorption rate in uncoated NPs to Néel relaxation and hysteresis losses whereas dipole-dipole interactions caused the lower SAR values.

For hyperthermia devices, a safe and effective external ac magnetic field is required to stimulate the implanted NPs. Here, the major issues are field uniformity, patient's convenience and proficiency of working for the whole body. Multi-turn inductive coils in the homemade devices discussed above serve the purpose for small animal preclinical trails. It is also worth to mention a magnetic ac hyperthermia (MACH) developed by Kallumadil [110] in response to the lack of adequate induction heaters available on the market that satisfy the criteria of producing large magnetic fields, being tuneable in frequency and practical in clinical applications. The inventors have been able to produce a variety of coil appendages that allow the MACH to deliver the inductive heating in various ways, highlighting the versatility of the machine, which is essential if taking this further to clinic and allows for self-tuning. The sample is placed in an Eppendorf (2 ml volume) inside the coil. Upon application of the frequency a temperature probe records the temperature increase of the solution over time. The MACH is still in development and currently on its $5^{th}$ generation [111]. Here, the novelty in the MACH is the use of the control circuit, the electronic breadboard, which generates high magnetic fields in a LC tank, where L is the inductor of the coil, and C the capacitor. The MACH was reported to operate at a fixed frequency of 1 MHz, however this frequency can be tuned using different LC. Besides the homemade, commercial devices are also available including the magnetherm by nanoTherics; the DM100, D5 series from nB Nanoscale biomagnetics; easyheat by Ambrell, or *in*

*vitro* magnetic field generator MGF1000 by European Institute of Science AB. These commercial devices have offered a range of variations in the ac magnetic field with varying frequency, amplitude, flux density to provide reliable and reproducible results for NPs heating. Real time tracking of heating measurement can be done using in situ set up of a pancake coil MACH hyperthermic system with a live –cell-imaging microscope (confocal microscope) [112].

**3. Photo-induced hyperthermia**

The use of radiative sources to induce hyperthermia have been established to treat surface lesions and tumors since the beginning of the 20$^{th}$ century. Initially radiative treatments were based on infra-red (IR) lamps and photosensitizer to induce thermal damage or oxidative stress on the affected areas of the patients, but they could only be applied on entire sections of the body and so it greatly increases the opportunity of collateral damage on healthy tissues and the stress on the patient. This technique is also called optical hyperthermia or sometimes, in modern aspect, it can be addressed as “laser hyperthermia” (Figs. 1b&c).

The use of NPs as localized sources of heat overcomes the aforementioned problem. Here, NPs can be tuned to be actively absorbing near IR wavelengths, where biological tissues have limited absorption, expanding the field of application of photo-induced hyperthermia to internal tissues and tumor mass instead of surface applications [113]. The intense absorption of these kind of particles compared with dyes and photosensitizers and their sharp absorption band allowed a greater efficiency on the energy conversion of the particles, either by surface plasmon resonance (SPR) or carbon reticle vibrational state relaxation, reducing the amount of energy necessary to trigger the hyperthermia effect and in consequences the collateral damage on the healthy tissues surrounding the tumor. The use of photoactivated NPs generates small

high temperature hot spots in direct contact with the tumor mass, in the area illuminated by the laser, focusing the hyperthermia effect on the target instead of relying on the heat diffusion of the tissue surrounding the tumor.

### 3.1. Mechanisms of Photo-induced hyperthermia

Light interacts with matter can be absorbed, transmitted or reflected. The absorbed part can be converted to heat while the reflected one scattered in the surrounding space. The interaction with nanomaterials is complex in which absorbed photons produce heat (emission of phonons) and are responsible for luminescence (emission of photons of different energies) as well. A large absorption efficiency and a limited emission yield are requirements in the selection of NPs in order to obtain a large light-to-heat conversion efficiency. In the following sections, light–matter interaction and different heat generating mechanisms occurring when a NP is illuminated by a light beam are described.

#### 3.1.1. Surface plasmon resonance absorption

When metal particles are reduced to a size comparable to the mean free path of the electrons in their conduction band, *e.g.* 40-50 nm for Au, they develop a strong absorption at some specific range of wavelength. This phenomenon is caused by the electrons on the surface of the material resonating on the entire length of the nanomaterial which generate a coherent motion called surface plasmon resonance (SPR) [114]. Depending on the geometry, orientation, and material, SPR leads to intense interactions of the particle with light within a range of optical frequencies. The periodic oscillation of the electrons is due to the difference between the length of the electrons mean free path and size of the particle which also determine its frequency [115]. These characteristics of SPR limit the interactions of NPs with light to specific

wavelengths, which resonate with the oscillating electrons. When the high-energy states generated by the oscillation decay, it releases the energy with non-radiative processes leading to increase of the temperature of the solution surrounding the particles. The connection between shape and size of metal NPs and their SPR is particularly evident for anisotropic NPs (as Au nanorods) for which the absorption peak of the lateral SPR can be tuned to specific wavelengths controlling the parameters of the synthesis (Fig.5a&b).

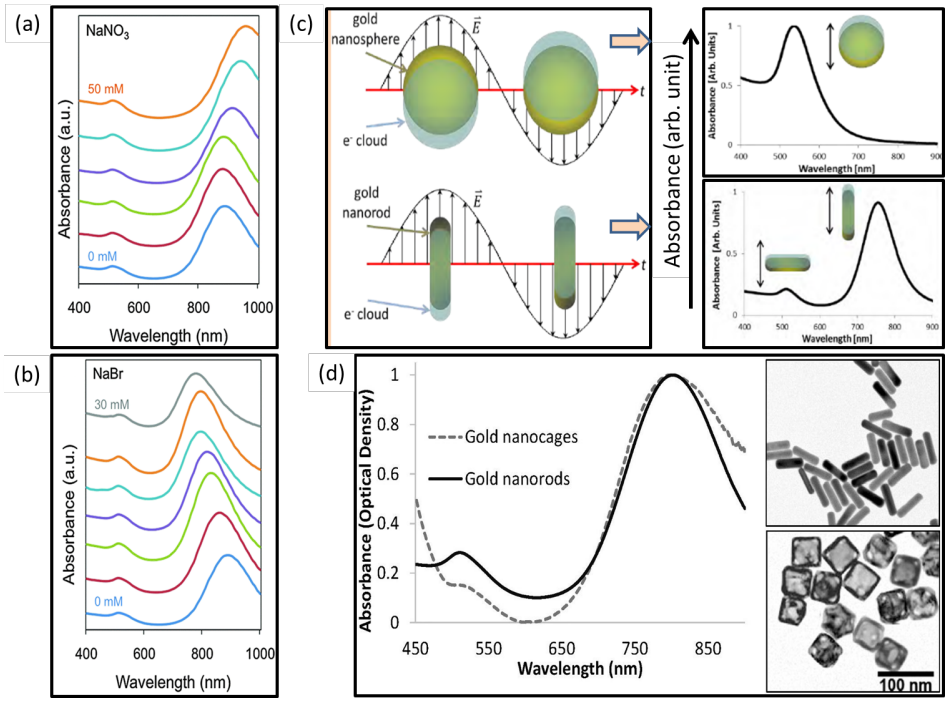


**Fig 5:** (a-b)Normalized extinction spectra of Au NPs grown in the presence of additional amounts of Hofmeister salts: for (a) the salt concentrations are 0 mM (blue), 10 mM (red), 20 mM (green), 30 mM (purple), 40 mM (turquoise) and 50 mM (orange) from bottom to top, and for (d) the salt concentrations are 0 mM (blue), 5 mM (red), 10 mM (green), 15 mM (purple), 20 mM (turquoise), 25 mM (orange) and 30 mM (grey), from bottom to top [116]. (c) Surface plasmon resonance in Au nanospheres and Au nanorods. (d) Au nanorods and nanocages absorbance spectrum (left), TEM image of Au nanorods (top right) with length and width of 60 × 14.8 ± 6.5 × 2.0 nm and TEM image of Au nanocages (bottom right) with edge length of 50 ± 7 nm, 100 nm. The scale bar applies to both TEM images [117]. (Reprinted with permission

from Refs. [116, 117]; Copyright 2016, The Royal Society of Chemistry & Copyright 2015, Elsevier Ltd., respectively)

The interaction of light with particles can be quantified by the scattering and absorption cross sections $C_s$ and $C_a$, respectively. The sum of these parameters is defined as the extinction cross section $C_e$. These values describe the area of light that interacts with the particle and they can be orders of magnitude smaller or larger than the geometric cross section of the particle.

For perfectly spherical nanospheres, Mie *et al.* [118] showed that these parameters can be calculated exactly by solving Maxwell's equations:

$$c_e = \frac{2\pi}{|k|^2}\sum_{L=1}^{\infty}(2L+1)R_e(a_L + b_L);$$

$$c_s = \frac{2\pi}{|k|^2}\sum_{L=1}^{\infty}(2L+1)(|a_L|^2 + |b_L|^2) \quad (11)$$

With $a_L = \frac{m\psi_L(mx)\psi'_L(x) - \psi'_L(mx)\psi_L(x)}{m\psi_L(mx)\eta'_L(x) - \psi'_L(mx)\eta_L(x)}$;

$$b_L = \frac{\psi_L(mx)\psi'_L(x) - m\psi'_L(mx)\psi_L(x)}{\psi_L(mx)\eta'_L(x) - \psi'_L(mx)\eta_L(x)} \quad (12)$$

where m is the ratio between the complex parameter describing their fraction of the particle and the real index of refraction of the surrounding medium, k the wave-vector, r the radius of the particle and η the Ricatti-Bessel cylindrical functions. The prime notation indicates differentiation with respect to the argument in parentheses. In general, for nonspherical particles, the cross sections must be determined with indirect measurements or with mathematical simulations, *e.g.* discrete dipole approximation (DDA) [119].

The above equations clearly state that the spectral shape and magnitudes of the cross sections depends on the geometry and the optical properties of the particle or the properties of surrounding material. A consequence of this dependence is that the optical properties of

metallic particles can be tuned to give a desired response at a particular wavelength. Metallic NPs, at their peak SPR absorption, can have optical cross sections orders of magnitude larger than their geometric cross sections [116]. Peak $C_a$ values can be 5 orders of magnitude larger than that in conventional absorbing dyes, and peak $C_s$ can be 5 orders of magnitude larger than fluorescence from strongly fluorescing dyes. Au nano-spheres with a diameter of 70 nm exhibit a peak SPR at 530 nm when suspended in water. Au nanorods with a length of 50 nm and a width of 15 nm exhibit two peaks when isotropically oriented in water, one at 510 nm when the electric field is parallel to the short axis of the nanorod and another at 780 nm when the electric field is parallel to the long axis of the Au nanorod (Fig. 5c).

**3.1.2. Interactions between light and carbon reticle vibrational state**

Delocalized carbon nanostructures can function as dark bodies and absorb a wide range of wavelengths, which is converted in vibrations of the C-C reticule and released as heat when the vibrational states decay [120, 121]. The photo-thermal properties of the materials depend on the regularity of their structure and from the amounts of impurities and dopants introduced in their reticule which can trigger other mechanisms of energy dissipation [121, 122].

**3.1.3. Generation of heat in nanoparticles: role of non-radiative recombination**

The radiation energy or optical energy may be transformed into several forms when light is being absorbed. A usual energy conversion process caused by the interaction of a material with light is the excitation of electrons which allowed the jump from lower energy state to the higher one without the generation of charge. In the relaxation from the excited state the electrons release energy in radiative or non-radiative form. Radiative relaxation releases energy in the form of photons causing spontaneous light emission (*e.g.* fluorescence or luminescence),

while non-radiative relaxation leads to generation of phonons which induce the increase of the vibrational state of the system and it converted into heat.

Laser or photo-induced hyperthermia applications have most of the research work at clinical level in case of plasmonic NPs, *e.g.* Au, Ag, Pd. Non-radiative transitions plays critical role in metal NPs upon light absorption where electric field component of irradiated light makes free electrons oscillate collectively within NPs which further collides with the nuclei and as a result energy is transferred into vibration modes of lattice transforming into heat. This process leads to plasmon resonance when irradiated light frequency matches with natural frequency of the free electron under interacting force of the nuclei. This is the main mechanism responsible for heat generation in metal NPs. Although Ag NPs generates roughly 10 times as much as heat compared to Au NPs at its plasmon resonance wavelength, Au is still favored in biomedical applications as agents for cancer therapy due to its chemical stability. The heat generation of several typical semiconductor QDs such as ZnS, ZnSe NPs is very low compared to that of Au. In the former, the heating mechanism is the generation of electron-hole pairs and the subsequent non-radiative recombination which is less efficient for heat conversion than the SPR of metal NPs.

Recently, $Fe_3O_4$ NPs are found to be most interesting not only for magnetic hyperthermia but also for photo-thermal hyperthermia. They have been observed displaying a photothermal effect which allows local environmental heating upon application of NIR laser [123]. The physical origin of this photothermal effect is important to understand. Iron oxides in the form of magnetite ($Fe_3O_4$), maghemite ($\gamma$-$Fe_2O_3$), and hematite ($\alpha$-$Fe_2O_3$) are abundant in nature. The optical properties of hematite were well investigated, and several theoretical and experimental

investigations reveal a band gap of 2.1–2.2 eV that has a potential application in the solar energy conversions. Magnetite is also a potential candidate due to its light absorption capabilities from visible to NIR range. Around 119 K, a Verwey transition from semiconductor to metal phase occurs leading to the change in optical and magnetic properties. $Fe_3O_4$ (chemical formula: $(Fe^{3+})_A[Fe^{3+}Fe^{2+}]_B(O^{2-})_4$) has an inverse spinel structure with face centered cubic (fcc) lattice of $O^{2-}$. Valence band of O(2p) to the empty conduction band of Fe(4s) in $Fe_3O_4$ is separated by 4-6 eV [123]. Fig. 6 explains the energy band gaping octahedral (B-site) and tetrahedral (A-site) due to the crystal field splitting.

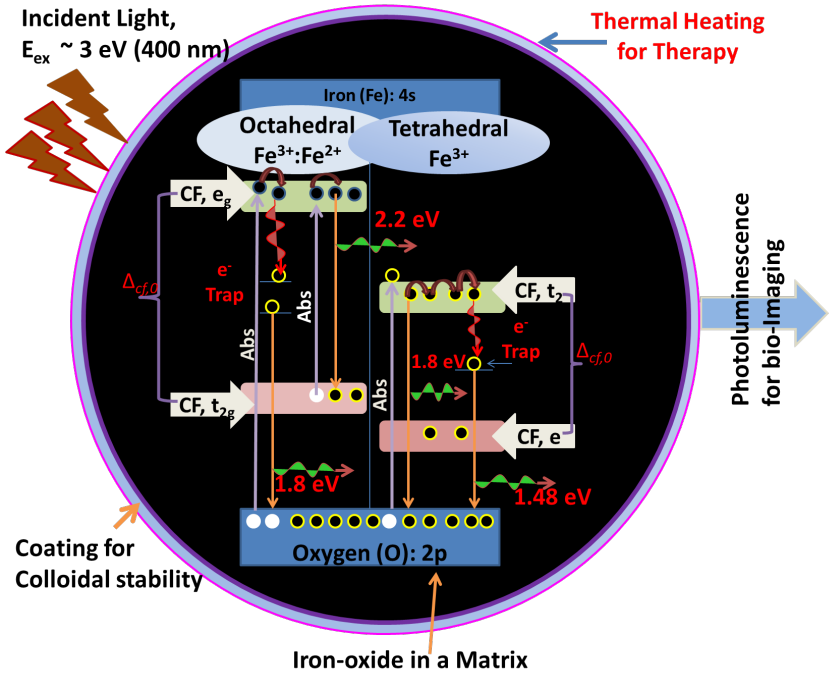


**Fig. 6:** Schematic representation of spatially confined $Fe_3O_4$ NPs embedded in an organic matrix (polystyrene matrix) and its energy bands.

Photoluminescence light emission from ultraviolet (UV) to NIR plays important role in photothermal applications and the excitation mechanisms can range from bound exciton in QDs to surface plasmon in metal NPs as stated earlier. Sadat *et al.* [109] prepared a variety of

different sized nanocrystals (10 nm–5 μm) and upon excitation with 407 nm laser, three emission peaks around 560 nm, 695 nm and 840 nm were observed. Cherepy *et al.* [124] observed transient absorption around the red-IR region. The short span "hot" electron model supported the explanation of the absorbed characteristics due to thermal radiation. It is possible to create mid-band gap states due to intrinsic defects and electrons transit through defects can be trapped there. Further electrons are relaxed to ground state emitting higher wavelength in IR region which is really independent on excitation radiation or energy of laser [124].

The observed photoluminescence peak around 560 nm (~ 2.2eV) can be assigned to $t_{2g} \rightarrow e_g$ on octahedral site due to the radiative recombination of mobile electrons and the peak at ~690 nm (1.79 eV) to (i) $t_2 \rightarrow O(2p)$ on tetrahedral site or (ii) the recombination of trapped electrons from the octahedral site to O(2p). The peak in IR region (845 nm, 1.47 eV) is due to transition of electron trapped on tetrahedral site created by oxygen vacancy. Coating materials also contribute their own characteristics. A polyacrylic acid coated iron oxide shows better photothermal conversion efficiency (76 %) as compared to polystyrene)/$Fe_3O_4$ (28 %), if excited at 785 nm. In addition, individually coated NPs experience more non-radiative recombination than embedded systems where collective intensity plays a role.

Cherepy *et al.* [124] investigated the photoexcited electron dynamics in ultrasmall (1–2 nm) γ-$Fe_2O_3$, commercial 50 nm diameter γ-$Fe_2O_3$, and spindle shape (1 × 5) nm α-$Fe_2O_3$ NPs. They found decay times of 0.36 ps (γ-$Fe_2O_3$), 4.2 ps (50 nm diameter γ-$Fe_2O_3$), and 67 ps (spindle shape α-$Fe_2O_3$) upon exciting by 390 nm, 150 fs excitation laser pulse with a 720 nm probe. This fast decay time suggests that relaxation of photoexcited electron is due to electron-hole

recombination which is bridged either by the intrinsic mid-bandgaps' states or trap-gaps due the internal defects. In other words, non-radiative mechanism can be a central theme among electrons and this mechanism can be inferred from several processes such as fast decay of electrons (excitation pulse and electronic transition in semiconductor), release of phonons instead of photons.

### 3.2. Parameters affecting the photo-induced hyperthermia

The ideal NPs for photo-induced hyperthermia need to be able to convert light into heat with a good efficiency. Here it is important that NPs can interact with NIR light to exploit the optical window of the human tissues. In addition, NPs should not be toxic, stable enough in biological condition to reach the target area tissues.

As shown in the review from Zhang *et al.* [125] the geometry of the particles used for hyperthermia is a fundamental parameter in controlling the interaction between light and NPs. Anisotropic NPs generate a more defined charge separation when their SPR is excited. The increase of intensity of SPR increases the amount of energy they can harvest from the light and consequently the amount of heat released [126]. Another way to increase the heat conversion efficiency is to form particles with cavities as Au nanoshells, nanocages or carbon nanotubes [26, 127].

Tuning the size of the particles is also an important factor in boosting the light-heat conversion. Particles of different sizes absorb different wavelengths and with a careful synthesis it is possible to match the absorption of the particles with the emission of the excitation light source to maximize the overlapping between the wavelengths [25]. An exception to the general requirements for photo-induced hyperthermia is the heat conversion of IONPs where the

thermal response or photothermal conversion efficiency is primarily due to electronic transitions between d orbitals of neighboring Fe ions within the lattice. Here, as long as the wavelength of laser irradiation is lower than that of IR, the mid-bandgap states trap the excited 'hot' electrons and produce phonons that are carriers of heat [128].

Effect of location of NPs is also important with respect to the cell in overall heating efficiency of photothermal treatment. Zhou *et al.* [129] performed *in vitro* experiments by analyzing efficiency of treatment for extracellular and intracellular therapies using light induced hyperthermia. For moderate continuous wave laser powers, the photothermal therapy was more efficient when the Au nanorods were attached to the cells than when the NIR thermal therapy outside the cells, *i.e.* in the bath solution around the cells to be treated (extracellular therapy).

In general, photothermal therapies use continuous or pulsed wave lasers as light sources. Mechanism of damaging cell due to photothermal effect is different in these types of lasers as they have different intensities, time profile. It is important to have optimum value of power density (intensity) and energy influence on the biosystem that depends on time of irradiation. For practical purpose, optimum intensity depends on cell type, photothermal agents, bio-environment etc. and the efficient photothermal treatment varies in the laser range from 1 to about 100 $W/cm^2$.

### 3.3. Potential photo-induced hyperthermia nanomaterial

Many kinds of nanomaterials have been studied for photo induced hyperthermia including Ag nanoprisms, Pd nanosheets, Au NPs and carbon nanostructures. The latter two are the most

suitable for hyperthermia because they have a well-known chemistry, inert in physiological conditions and being in different shapes.

### 3.3.1. Carbon Nanostructures

Carbon nanostructures, containing delocalized c-c backbone, have been extensively studied. These materials have potential applications in nanomedicine because of their characteristic opto-electronic properties and biofunctionalization. Carbon sheets are composed of a single molecule of graphene which extend for hundreds of micrometers of surface but only one atom of thickness. Graphene is the constituent unit of graphite and the main natural form of elementary carbon. Here, graphene can be produced in bi-dimensional sheets and reduced to nano-sized fragments by sonication [130]. The fragments obtained by sonication can be used as support for other moieties as mesoporous silica or oxides. The highly delocalized electronic structure can absorb a wide range of wavelengths and to release the energy absorbed as heat. Carbon nanotubes are micrometer long tubular carbon structures [127]. They can be composed by a single sheet of graphene closed to form a cylinder (single wall nanotubes) or by multiple concentric surfaces (multi walled nanotubes) [120]. Depending on the symmetry of the graphene sheet, which forms the tube, carbon nanotubes can possess electrical and thermal properties that can vary from metallic to semiconductive [131]. Their electronic structure is delocalized on the entire molecule and allowed to absorb a wide range of wavelengths, which get converted in vibrational energy. Carbon nanotubes have an impressive light to heat conversion capability (20 °C of $\Delta$T for 5 min of exposure to 0.7 W/cm$^2$ of a solution 50 nM) [127] but they have been limited in actual applications for clinical studies due to concerns about toxicity [132, 133].

Fullerene are spherical structures of sixty carbon atoms formed by a single sheet of graphene closed on itself. These kinds of NPs are composed of atoms covalently bounded together and they are on the threshold between macromolecules and NPs. Since this large delocalized system has an electronic behavior similar to a metal NPs, it has been commonly studied for opto-electronic applications. Recently it has been reported that hydroxy-modified fullerene can generate intense heat if exposed to 785 nm laser light for few minutes and can be applied to biological systems [134].

**3.3.2. Au nanomaterials**

Au nanomaterials have been studied extensively since they possess interesting properties that make them suitable for specific applications such as carrying active substances inside tumors, antenna for radiotherapy, to track the uptake of drugs or for direct hyperthermia [135,136]. Spherical Au NPs can be synthesized with a good degree of reproducibility having a strong absorption at 520 nm that shift towards red when the particles are close enough to share the plasmonic resonance or when their size is above 100 nm in diameter [137]. Au nanorods are bi-dimensional structured possessing two SPR peaks of absorption: the first peak is generated by the transverse SPR of the shorter side of the rods having absorption close to 520 nm, and the second longitudinal SPR peak which can be tuned from 650 nm to 1200 nm depending on the length of the rod and its ratio between long and short dimensions (Fig. 5d) [138]. Au nanorods have higher energy conversion efficiency than spherical NPs and their characteristic double peak absorption can be used to combine imaging, drug delivery or hyperthermia with promising results *in vitro* and *in vivo* [139]. Au nanocages are nano-sized cubic crystal with a certain percent of cavities inside their structure (Fig.5d), *e.g.* a sponge like mesh or a frame containing

an empty space. The optical properties of the nanocages are determined by the lateral size of the cube shape and the ratio Au/cavities [140]. The hollow structure of the nanocages made them a good candidate for drug encapsulation. At the same time, the tunability of their SPR allowed them to be used as sensor or sources of hyperthermia.

Au nanoshells are characterized by a central core of dielectric material such as silica or ZnS surrounded by a thin layer of Au. The absorption of light on the nanoshells is determined by the thickness of the Au layer and the size of the core. Since Au nanoshells with silica core have a strong absorbance in the NIR region and a good capability to generate heat, they have been tested as a source of hyperthermia for tumor ablation in mice [141]. Au nanostars are a class of anisotropic nanostructures characterized by a central core from which it departs some spike-like structures. The shape, number and the length of the spikes depend on the synthesis and it can vary from few short and thick prism points to numerous needles like protrusions. The peculiar structure of this class of NPs generates a characteristic SPR effect having a broad and intense light absorption in the visible and IR region and two defined sharp peaks related to the SPR of the core and the spikes [142]. This kind of Au nanostars have been intensively studied recently for their role in Raman enhancement and the elevated extinction coefficient in the IR region that make them promising candidate for hyperthermia applications as well as treatment of difficult to reach areas of the human body such as brain tumor.

**3.3.3. Iron oxide nanoparticles (IONPs) and Ferrites**

Water soluble PEGylated (where PEG is polyethylene glycol)MNPs (PEG–$Fe_3O_4$) prepared with a one pot solvothermal method were observed to be able to rise the temperature of a solution to 47.8 °C from room temperature after 10 min of laser irradiation at 808 nm (2 W/$cm^2$)for a

concentration of 1 mg/mL [143]. In another work, Chu *et al.* [144] prepared IONPs (~ 9.1 nm) coated with carboxyl-terminated poly (ethylene glycol)-phospholipid and– dispersed in phosphate-buffered saline (PBS) and tested for the *in vivo* and *invitro* experiments using photo-induced thermal treatments. Samples were irradiated for 20 min using 808 nm laser (0.25 $W/cm^2$) and the cell viability decreased significantly to 52 % of the original value. A higher concentration (8 mg/mL) was injected in nude mice to test and treatment was continued for 20 days. As a result, tumor growth was inhibited. Similar results were observed by tuning shape and size of IONPs [145]. IONPs synthesized using hydrothermal route may require high intensity to increase temperature in an *invitro* experiments where 785 nm laser (5 min, 3.75 $W/cm^2$) was used to increase the temperature by 7-8 $^oC$ [146]. Highly crystalline IONPs can increase temperature up to clinical relevant temperature (40 – 50 °C) after 10 min of exposition to a 2 $W/cm^2$ laser (808 nm) [145, 147], when applied to *in vivo* or *in vitro* experiments. IONPs can also be synthesized by biological routes using magneto-tactic bacteria for the treatment and control of tumors in mice [148].

Alternatively, to Au and C, a variety of nanostructures containing metals have been tested for hyperthermia. Pd nanosheets having hexagonal tiles between 20 and 60 nm long and less than 10 atoms in thickness produce a strong extinction coefficient in the IR region (800 – 1050 nm) and they can be used to increase the temperature of a solution to 20 °C above the room temperature in 10 min of laser (808 nm, 1 W) exposure [149, 150]. Copper sulphate or Se nanocrystals have low toxicity and a high efficiency in converting NIR radiation into heat. The activity of these nanocrystals has been tested *in vivo* on mice inoculated with human cervical

carcinoma, showing a heat conversion efficiency of 25.6 % and complete ablation of the tumor in 7 min of IR laser exposure (0.51 W/cm$^2$) [151, 152].

### 3.3.4.Quantum Dots (QDs)

QDs are semiconductor bandgap light-emitting nanomaterials (*e.g.* CdSe, CdTe, PbS, InAs, InP, ZnSe with size less than 2-10 nm and their optical properties can be used for theranostic applications. In order to enhance the efficiency of QDs, sometimes core-shell (*e.g.* CdSe/ZnS) engineering is adopted [153] that provides the exciton confinement and minimize surface defects. In this core/shell structure it showed size dependent emission spectra upon excitation which can be tuned from UV to IR by increasing the core size to provide a redshift of the spectrum. The most popular synthesis of QDs is based on the high-temperature decomposition of organometallic precursors in the presence of surfactants and organic solvents with high boiling point. There are several reasons that make QDs potential fluorescent nanomaterial, such as a high quantum yield, narrow fluorescence band, broad excitation spectrum, excellent photostability, long fluorescence lifetime, and large Stokes shift. These remarkable photophysical parameters of QDs led to their broad recognition in the life sciences such as discrete biological events, tracking cell migrations, detection of pathogens and whole-animal imaging and therapy [154]. Gao *et al.* [155] have developed cancer-targeting theranostic QDs by coating core-shell CdSe-ZnS QDs with amphiphilic polymer and attaching a tumor binding ligand to the nanocomposite. The designed multifunctional QDs demonstrated successful recognition of *in vivo* tumor by the passive labelling via EPR effect and by the active targeting to the cancer-specific biomarkers. The cytotoxicity and the physicochemical properties of QDs depends on several factors including size, particle charge, stability, surface coatings, the

dosage, exposure concentration and the route used to administer. In order to reduce the cytotoxicity, it was to coat the toxic core with a protective ZnS layer, cap it with bio-safe PEG polymers or replace the toxic elements with non-toxic components [156]. Nonetheless, the metabolism and degradation of QDs within the body is still largely unknown and the associated toxic hazard remains a limitation for the usage of QDs in biomedical applications. Fluorescent QDs (tailored from UV to IR) can be used for photo-induced therapy and are capable of intracellular thermal sensing during hyperthermia treatments.

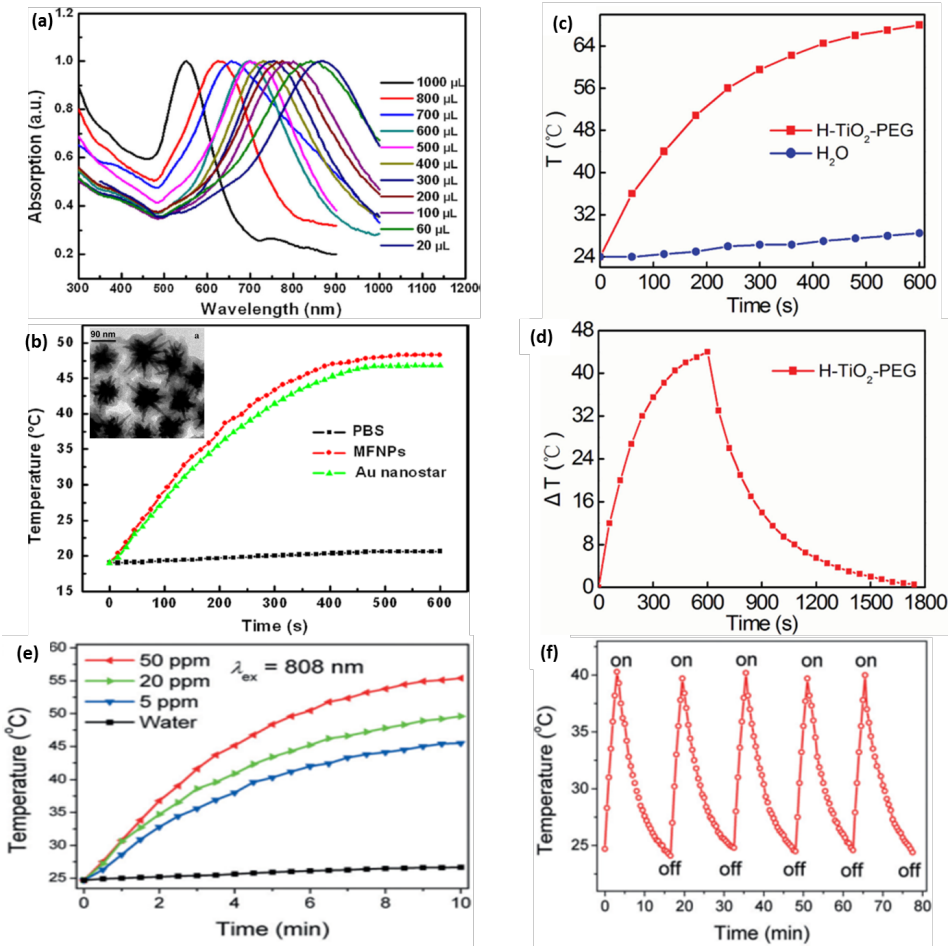


**Fig 7:**(a) Normalized extinction spectra of the star solutions of Au nanostars/QDs-doped $SiO_2$ NPs (TEM image in inset) with various seed volume from 20 to 1,000 µL, (d) The temperature elevation of the aqueous dispersion of different samples, Au stars, and PBS under 808 nm laser at 1 W/cm$^2$ for 10 min [157]; c) Temperature evaluation of H-$TiO_2$-PEG NPs (100 µg/mL ) and

pure water with 808 nm laser irradiation at 2 W/cm$^2$ for different times, d) The temperature change (ΔT) response to NIR laser on and off in period of 2,100 s [158], e) Photothermal heating curves of pure water and PEG modified BPQDs dispersed in water at different concentrations under irradiation with an 808 nm laser (1.0 W/cm$^2$), f) Heating of a suspension of the PEG-modified BPQDs in water for five laser on/off cycles [159] (Reprinted with permission from Ref. [157], Copyright 2014, Springer; & Refs. [158, 159], Copyright 2015, John Wiley& Sons)

Cu-based semiconductors (*e.g.* CuSe, CuS) have attracted great attention showing two absorption peaks: one in the NIR and another in UV region. The explanation behind the existence of these two peaks are controversial and these QDs showed metal-like absorption behavior [157]. Several results suggested that optical excitation of Cu-based QDs produces phonon-assisted heating (electronic decay or relaxation of free carrier surface currents). Yin *et al* reported a novel class of cell probe structured as Au nanostar@$SiO_2$@CdTeS,QDs@$SiO_2$ nanoprobes, (size ~ 129 nm, Fig. 7, inset 7b ) and demonstrated photothermal properties [157]. The fluorescence signal of QDs was enhanced 23% more in this new material, compared with the pure QDs (Fig. 7a). The *in vitro* study showed that the magnetic fluorescent NPs can realize the targeted labeling after functionalized with anti-body. Furthermore, the nanoprobe displays strong surface plasmonic resonance absorbance in the NIR region, thus exhibiting an NIR (808 nm)-induced temperature elevation. The temperature of magnetic fluorescent NPs solution increased significantly under constant irradiation, which is high enough to destroy the targeted cancer cell. From the flow cytometry graph, over 99.8 % of SK-BR-3 cancer cells lost their cell viability after irradiation for 10 min at a power density of 1 W/cm$^2$ (Fig. 7b). The multifunctional NPs are expected to serve as luminescent markers while attached to bioligands and are capable of being used to destroy the target cancer cell.

White $TiO_2$ NPs have been widely used for cancer photodynamic therapy based on their ultraviolet light–triggered properties. On the other hand, hydrogenated black $TiO_2$ (H-$TiO_2$ ) NPs with near IR absorption was also explored as photothermal agent for cancer therapy to circumvent the obstacle of ultraviolet light excitation [158]. Here, it was shown that photothermal effect of H-$TiO_2$ NPs can be attributed to their dramatically enhanced nonradiative recombination. After PEG coating, H-$TiO_2$-PEG NPs exhibit high photothermal conversion efficiency of 40.8 %, and stable size distribution in serum solution (Figs. 7 c&d).The toxicity and cancer therapy effect of H-$TiO_2$-PEG NPs were evaluated *in vitro* and *in vivo* in which it was found NPs exhibit low toxicity, high efficiency as a photothermal agent for cancer therapy and they are promising for further biomedical applications [158]. To explain, the laser excitation and further temperature change of NIR irradiated tumor, photothermal imaging of tumor-bearing mice was measured. It was showed that NIR-triggered cancer photothermal therapy of H-$TiO_2$ has better applicability than UV light–induced photodynamic therapy of $TiO_2$ and thus can advance the applications of $TiO_2$ in biomedicine in the future.

Sun *et al.* [159] demonstrated black phosphorus QDs (BPQDs) synthesized using a liquid exfoliation method combining probe sonication and bath sonication. With a lateral size of approximately 2.6 nm and a thickness of about 1.5 nm, the ultrasmall BPQDs exhibited an excellent NIR photothermal performance with a large extinction coefficient of 14.8 L/molcm at 808 nm, a photothermal conversion efficiency of 28.4 %, as well as good photostability (Fig.7e&f). NIR photoexcitation of the BPQDs in the presence of C6 and MCF7 cancer cells led to significant cell death, suggesting that the NPs have large potential as photothermal agent. After PEG conjugation, the BPQDs showed enhanced stability in physiological medium and there was

no observable toxicity to different types of cells. NIR photoexcitation of the BPQDs in the presence of C6 and MCF7 cancer cells led to significant cell death, suggesting the potential PTT applications of the NPs (Fig. 7 e&f). Owing to their ultrasmall size, the BPQDs have a long blood circulation time, enabling the attachment of additional nonimmunogenic or cellular targeting molecules for targeted photothermal cancer therapy.

Ding *et al.* [160] realized photoacoustic imaging-guided photothermal/photodynamic combined cancer treatment just via a single material, $MoO_{3-x}$ QDs. Due to their strong NIR harvesting ability, $MoO_{3-x}$ QDs can convert incident light into hyperthermia and sensitize the formation of singlet oxygen synchronously as evidenced by *in vitro* assay, hence, they can behave as both photothermal and photodynamic agents effectively and act as a "dual-punch" to cancer cells. $MoO_{3-x}$ QDs exhibited strong optical absorption in the biological window and a high photothermal conversion efficiency of 25.5 % under 880 nm laser irradiation. Benefiting from this, $MoO_{3-x}$ QDs produced local hyperthermia upon irradiation *in vitro* or at the tumor site *in vivo*, thus realizing the photothermal treatment outcome. Meanwhile, a non-fluorescent probe result revealed that NIR light triggered $MoO_{3-x}$ resulted in an intracellular generation of singlet oxygen, producing photodynamic efficacy.

**3.3.5.Rare-earth containing NPs**

Rare earth ions-doped photoluminescent NPs (Ln NPs), have attracted a growing interest in biomedical applications [161]. Such NPs are considered to have better luminescence characteristics compared to QDs/dyes due to high photo and chemical stability, narrow and sharp 4f-4f emissions, a large Stoke and anti-Stokes shift, weak background autofluorescence and low biotoxicity. Depending upon the dopants, host, excitation and material engineering

(*e.g.* core-shell) a wide range of emission color tuning is possible. The biggest challenge in using these rare-earth doped NPs in biomedicals is their inherently excitation bands which can limit tissue penetration depth and local laser heating in biological samples [161].

Recently, the 808 nm-excited Ln NPs (absorption coefficient 0.02 $cm^{-1}$ at 808 nm, and 0.48 $cm^{-1}$ at 980 nm) and $Nd^{3+}$ dopant have received much attention in the fields of chemical and biomaterial science [162]. Here, higher quantum yields for 808 nm-excited LnNPs can be obtained owing to their large absorption cross section and/or high energy transfer efficiency. Consequently, these LnNPs are more appropriate for *in vitro/in vivo* biomedical applications, especially for experiments that require higher power density and longer-term excitation. So far, various kinds of 808 nm-excited LnNPs have been extensively reported and some researchers even regard 808 nm-excited LnNPs as the next generation of nanophosphors to be used in current diagnostic and theranostic applications. Herein, three main underlying principles for improving the quantum efficiency of LnNPs have been proposed [163,164]: i) reasonable design of core–shell structures, ii) surface-plasmon coupling, and iii) organic dye-sensitized LnNPs. The $1^{st}$ and $3^{rd}$ options are largely cited and well proved but not with the option $2^{nd}$. By storing a fraction of their energy in electron gas, surface plasmons are highly effective in creating a strongly localized and intense optical field, which enhance a variety of optical processes such as surface enhanced Raman scattering. In recent years, with the development of LnNPs, many researchers have concentrated their efforts on incorporating plasmonic nanostructures with LnNPs to boost the efficiency of the energy conversion process up to several hundred times. Chen *et al.* [165] reported a 9-fold up conversion luminescence enhancement by synthesizing $Nd_2O_3$/Au nano-composites through a co-precipitation process, while Li *et al.* [163] successfully

synthesized a core/shell/shell nanocomposite of $NaYF_4$:Nd,Yb,Ho@$SiO_2$@Ag by a physical conjugating method to obtain Ag-enhanced up conversion luminescence intensity with an enhancement factor of 15. Several theoretical and experimental studies on the mechanisms of plasmon luminescence enhancement have been carried out. Generally speaking, surface plasmon can influence the luminescence of LnNPs in three ways [166]: i) enhancing the absorption of the sensitizer through electric field coupling, ii) improving the radiative decay rate of the activator, and iii) increasing energy transfer from the sensitizers to activators. Even so, a complete understanding of the complex dynamics of luminescence under plasmonic fields needs further elucidation. The major difficulties lie in the multiple steps of the luminescence processes and the wide variations in geometry and excitation conditions [167].

NP-mediated PTT systems, which rely on generating heat to burn cancer cells, constitute a flexible, highly selective, cost effective, and accurate tool for cancer treatment. For $Nd^{3+}$-doped NPs, heat is normally produced as a result of multiphonon relaxation from the $Nd^{3+}$ excited states, or emission quenching effects mediated by closely located nonradiative centers [168]. Normally, when the concentration of $Nd^{3+}$ ions is high, the distance between neighboring $Nd^{3+}$ ions is reduced, resulting in the activation of nonradiative cross-relaxation mechanisms. In this case, the absorbed 808 nm NIR power is increased, while the NIR fluorescence efficiency is reduced, generating heat. In the last few years, researchers have tried to simultaneously achieve $Nd^{3+}$ luminescence and heat generation by experimentally determining a preferred $Nd^{3+}$ concentration inside the LnNPs, such as α-$NaYF_4$ colloidal and ultrasmall $NdVO_4$ NPs [168]. In this way, the NIR luminescence signal presented by these NPs can be applied not only to

determine the NPs location after their injection but also to monitor the post treatment evolution of the tumor itself and the biodistribution/clearance of the NPs from the body.

Apart from the bifunctional luminescent, $Nd^{3+}$ ions can act simultaneously as an imaging probe and photothermal agent owing to their unique achievement of real time control during PTT to keep collateral damage at a minimum. To construct this kind of NP, one direct way is to combine two nanosized elements into a single nanostructure: one acts as nano-heater and the other provides thermal sensing capacity. Some researchers also developed a strategy to integrate 808 nm-excited LnNPs with other kinds of PTT agents, such as Au, CuS NPs, indocyanine green (ICG), or polydopamine (PDA). Rocha *et al.* [168] successfully encapsulated Au nanorods and $LaF_3$:Nd NPs into single poly(lactic-co-glycolic acid) capsule having thermally monitoring subcutaneous PTT. However, this kind of "double particle" approach increases the complexity and instability of the system. To improve it, the design and synthesis of a single NP capable of both heating and thermal sensing appears to be especially interesting. Fortunately, by using $Nd^{3+}$-doped NPs, it was found possible to perform *in vivo* efficient temperature-controlled PTT of cancerous tumors. A systematic work was carried out by Carrasco *et al.* [169] with $Nd^{3+}$ doped $LaF_3$ biocompatible NPs to act at the same time as NIR light excited nano-heaters and fluorescent thermal nanosensors, based on particular excitation and de-excitation features of the $Nd^{3+}$ ions. The results showed that non-invasive intratumoral temperature readings during hyperthermia treatment are possible from a simple analysis of the intratumoral fluorescence generated by the $Nd^{3+}$doped $LaF_3$ NPs.

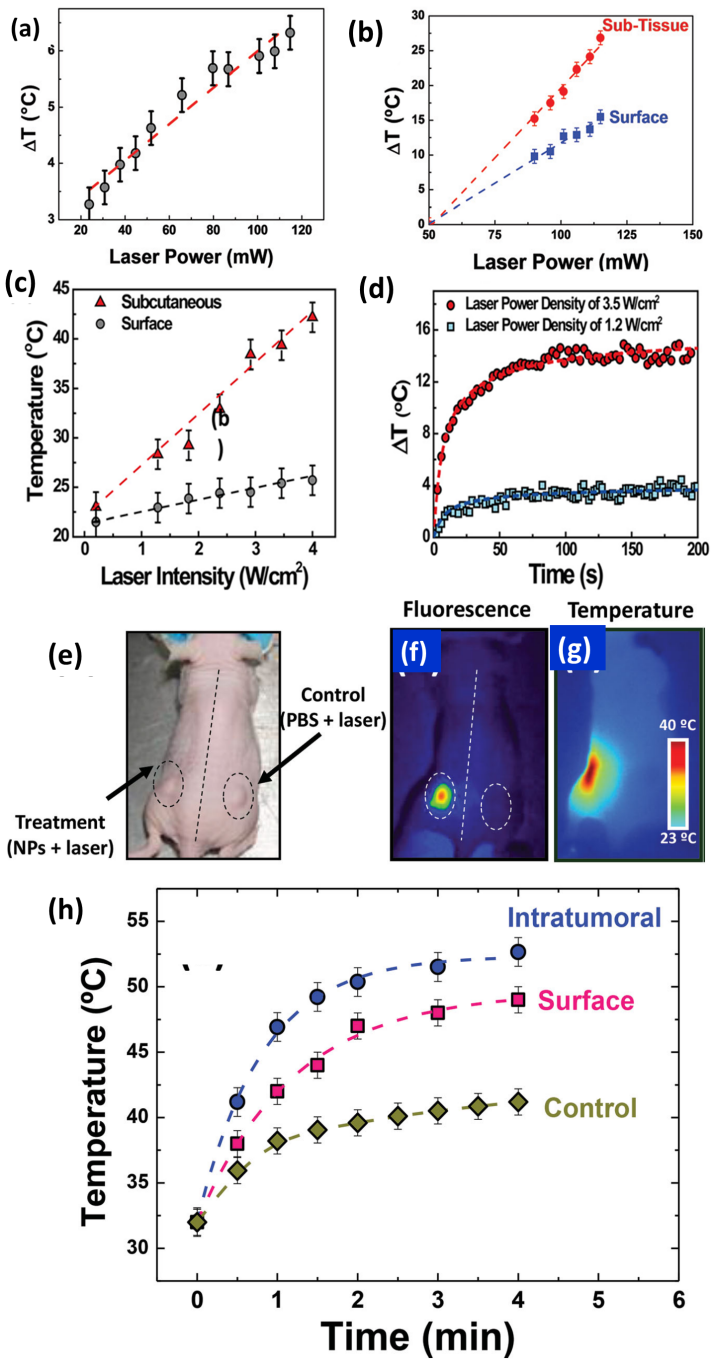


**Fig. 8:** (a) On-focus temperature increase in the aqueous solution as a function of the 808 nm laser power. (b) Surface and sub-tissue temperatures as obtained for different 808 nm laser powers [170]. c) Surface and subtissue temperatures as obtained for different 808 nm laser power densities. (d) Temperature stabilization of a tissue when exposed to an incident 808 nm laser beam at constant power density (1.2 W/cm$^2$ (blue) and 3.5 W/cm$^2$ (red) [171]. (e) Optical

image of a representative mouse with two tumors. A solution of "dense" Nd:$LaF_3$ NPs was injected only in the left-side tumor whereas the right-side one was used as a control. f-g) IR fluorescence and thermal images of the same mouse under 808 nm (4 W/$cm^2$) laser irradiation, respectively. The images show the fluorescent and heating signals differentially emitted by the treated tumor. h) Time evolution of the temperature at the tumor surface as obtained from the analysis of IR thermal images. The time evolution of intratumoral temperature obtained from the analysis of sub-tissue fluorescence is also included [169]. The dots are the experimental data and dashed lines are the linear fits.(Reprinted with permission from Ref. [169] Copyright 2015, John Wiley & Sons; Ref. [156], Copyright 2016, The Royal Society of Chemistry; & Ref. [171], Copyright 2016, AIP Publishing)

Ximendes *et al.* [170] demonstrate how single core/shell dielectric NPs with a highly $Nd^{3+}$ ion doped shell and an $Yb^{3+}$, $Er^{3+}$ co-doped core capable of simultaneous thermal sensing and heating under an 808 nm single beam excitation (Fig. 8 a&b). The spatial separation between the heating shell and sensing core provides remarkable values of the heating efficiency and thermal sensitivity, enabling their application in single beam-controlled heating experiments in both aqueous and tissue environments.

Further, Ximendes *et al.* [171] reported $Nd^{3+}$ and $Yb^{3+}$ doped $LaF_3$ (core-shell engineering) NPs capable of subcutaneous heating and thermal sensing under single beam 808 nm excitation. Efficient light-to-heat conversion is produced at the $Nd^{3+}$ (phonon-assisted relaxation to the metastable $^4F_{3/2}$) highly doped shell due to non-radiative de-excitations which becomes dominating if $Nd^{3+}$ concentration is higher, and shell is more efficient heating unit (Fig. 8 c&d). A phonon-assisted cross relaxation along with energy migration to killer impurities helps in the heating process. In Fig. 8c, the steady state subtissue and surface temperatures were recorded for different 808 nm power densities and in both cases, a linear relationship was experimentally

found. Fig. 8b shows the time dependence of the subcutaneous temperature variation under two different excitation laser power densities, obtained computing the time evolution of the intensity ratio from the subcutaneous emission spectra.

It should be noticed that the dynamic thermal reading demonstrated in Fig. 8b was obtained using the same NPs that were inducing the subcutaneous heating. In one representative example, Su *et al.* [166] reported a carbon-coated $NaLuF_4$:Yb/Er@$NaLuF_4$ core–shell up conversion nanocomposites which were useful for real-time monitoring of microscopic temperature in PTT. Carrasco *et al.* [169] demonstrated that thermally controlled therapy is possible by using $Nd^{3+}$ ion-doped $LaF_3$ nanocrystals. These NPs are capable of *in vivo* photothermal heating, fluorescent tumor localization and intratumoral thermal sensing. In Fig. 8e, these NPs in PBS buffer solution (Fig. 8f, bright) were injected in the left tumor and an equivalent PBS volume was injected in right side tumor for controlling and monitoring (Fig. 8f, no intensity). A laser (808 nm, 4 W/$cm^2$) was irradiated on both side (Fig. 8c), and as a result simultaneously monitoring the intratumoral and the surface temperature in left side tumor was possible during different time span of irradiation. The temperature versus time analysis is shown in Fig. 8h where temperature is stable in tumor (20 % higher than surface temperature) and at surface after around 3 min of the beginning of treatment.

### 3.4. Instrumentation for photo-induced hyperthermia

Contrarily to hyperthermia techniques photo-induced hyperthermia does not require complex machinery other than a NIR laser with intensity sufficient to activate the hyperthermia process. The selection of the excitation laser to NIR is limited by the opacity of the human tissues to most of radiation spectra resulting in viable range of wavelength in optical window between

780 – 1100 nm. Here, ideally the laser should transfer maximum energy to the particles in the tumor without damaging the surrounding cells. Control the collateral damage is an issue when using an external light source because the laser is forced to pass through all the tissues between the skin and the tumor. The general practice to overcome this problem is to deliver the laser light through an optical fiber insert in patient in direct contact with the area of application and using a terminal lens at the end of the fiber to defocus the laser in a small light brush quickly dissipating after few centimeters from the end of the fiber. The power of the laser source, the extension of the light brush (surface illuminated by the laser) and time of exposure are all factors that must be balanced in order to increase the efficiency of the thermal therapy reducing the secondary damages and it requires a great amount of repetitions to reach the optimal conditions (Fig. 1d) [11]. There are two main light sources commonly used in hyperthermia (Fig. 1b): diode lasers and Nd:YAG. These laser sources are commercially available and they can be tuned to excite a range of wavelength in the NIR. An important factor when choosing a laser for hyperthermia is the modality of emission, a laser can be emitted as continuous wave or as femtoseconds pulses. The former has relatively low intensity but can be applied continuously for minutes, while the latter has very high intensity, but it can only be administered in short flashes for a short time. Both modalities have their own advantages: the long exposure time of the continuous wave lasers increases the efficiency of the hyperthermal therapy, by increasing the time the activate particles interact with the tumor, while the femtoseconds pulse lasers generate instantaneously high energy hyperthermia points that can overcome the capability of the tumor to activate heat-resistance defense mechanisms [172]. The different modalities bring also different problems: long exposure increases the possibility of

damaging the tissues around the tumor, while the femtoseconds pulse laser needs multiple applications because the laser can be used only for few seconds each time [173].

**4. Comparison between magnetic and photo-induced hyperthermia and their combinatorial effect**

Classical methodology for the treatment of cancer are effective but presents serious problem of toxicity damaging healthy cells and DNA which may cause secondary tumors. Hyperthermia driven by nanomaterials have been used for a more precise strategy with interesting results for a wide variety of materials and shapes against cancer cells. Besides generating heat, functional NPs can also be targeted to the tumor to release active drugs when it is triggered by an external stimulus.

The MHT or PTT to generate hyperthermia has its own advantages and drawbacks compared one to another. PTT can achieve high temperature with the exposure to low laser intensity for short amount of time or with the brief exposure to a high energy pulsed laser. The materials used for the light-heat conversion generally have high conversion rates, but the efficiency is limited to the capability to carry the light in the effective range of the particles. Using the optical window of living tissues (780 – 1100 nm), the actual capability of penetration inside the body is below a centimeter, and the use of intense light sources would damage the light penetrated tissues. On the other hand, MHT has lower heat conversion but the use of magnetic fields to generate heat is an advantage since it virtually does not harm the body. Materials used for PTT (*e.g.* Au, Ag, carbon structure) are fairly inert in biological conditions and generally possess a well-known chemistry while for MHT, it requires a higher degree of control during the synthesis to obtain safe MNPs (*i.e.* stabilization, control on the impurity, passivation). Here, the

MNPs can be driven to the target by the same magnetic field used for the activation and they can be used as contrast agent of MRI [174, 175].

To maximize the benefits from the different techniques and to limit the drawbacks it is useful to create materials which can be used by both the magnetic and photo-induced hyperthermia. It was reported of some nanostructures which can be heated to trigger the release of a toxic payload in the area surrounding the tumor, and in this case, it is not required intense photo-induced energy sources damaging to the healthy tissues. In addition, it was also reported of materials that can be tracked by optical analysis or magnetic resonance and activated by a different stimulus, allowing the material to be used as a diagnostic device and therapeutic tool [12, 14, 102]. The development of a system be use for PTT and MHT together requires a great degree of control in the synthesis of magnetic and plasmonic materials. In this structure, it is generally a one-pot synthesis of the NPs followed by a post synthesis modification to reduce the toxicity and add functionalization. Most of the multifunctional materials have been tested only *in vitro* and the materials involve new branches of physics such as magneto-plasmonic, magnetic-luminescence, and magneto-photo thermal.

Recently, Ortegies *et al.* [176] reported the realization of an optomagnetic nanoplatforms which is able to generate heat using MHT and to emit in the NIR to allow the detection of the particles and a direct measurement of the progress of the heating process. The thermal control on the MHT process was achieved doping Nd SPION particles with $LaF_3$ which is luminescent in temperature range of 20–60 °C. Fig. 9 summarizes the heating results which show the optomagnetic hybrid nanostructures (OMHSs) developed a robust multifunctional platform, capable of fully controlled subcutaneous heating by using either optical or magnetic

stimulation. The potential of these materials was demonstrated by an *ex vivo* intracoronary heating experiment in which subtissue remote heating with contactless thermal feedback was successfully achieved.

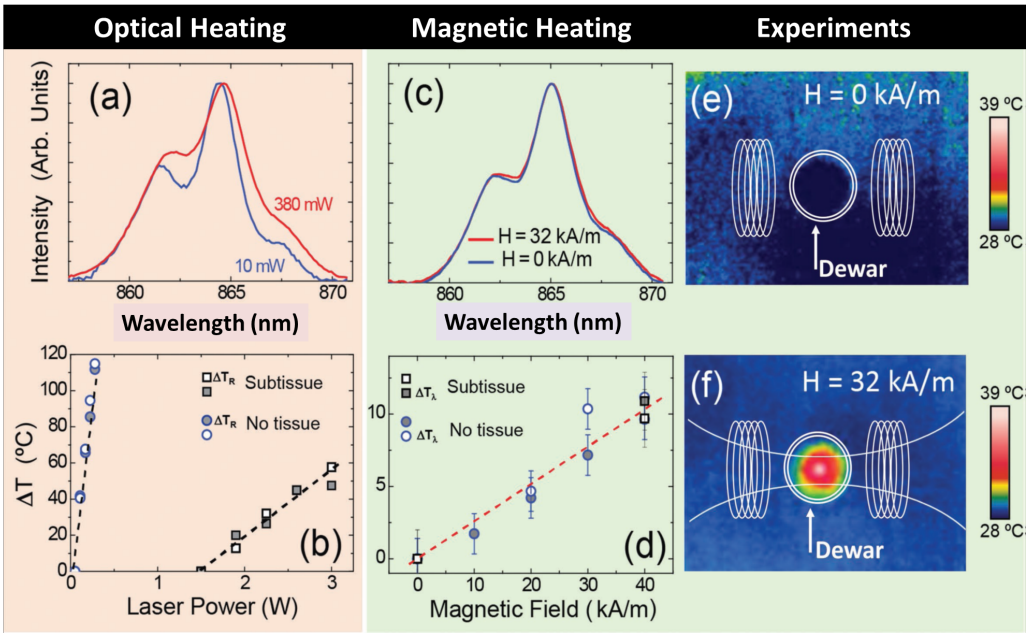


**Fig. 9:** a) Emission spectra generated by the OMHSs as obtained for two different laser powers: 10 mW (blue line) and 380 mW (red line). b) Temperature increment induced in the optically excited OMHSs as a function of the laser power obtained from the ratiometric ($\Delta T_R$) and spectral ($\Delta T_\lambda$) shift calibration in presence (circles) and absence (square)of tissue, respectively. c) Emission spectra generated by the OMHSs obtained in the absence (blue line) and presence (red line) of an ac magnetic field (100 kHz and 32 kA/m). d) Temperature increment induced in the OMHSs as a function of the applied magnetic field in the presence and absence of tissue with calibrations. e) Thermal image of the quartz tube containing the OMHSs in the absence of $H_{ac}$. f) Thermal image of the tube containing the OMHSs in the presence of $H_{ac}$ (100 kHz and 32 kA/m) [176]. (Reprinted with permission from Ref. [162], Copyright 2018, John Wiley & Sons)

Espinosa *et al.* [14] prepared iron-oxide nanocubes able to generate hyperthermia effect when activated either individually by a 808 nm laser and powers ranging from 0.3 to 2.5 W/cm$^2$, as

well as an ac magnetic field at frequencies of 110, 320, 520, 700, and 900 kHz; amplitude in the range of 12−25 mT (9.572 -19.943 kA/m) or to a dual combination of the two (Fig. 10). The system was tested for different concentrations and when exposed to increased laser intensity it showed remarkable consistent capability to rise the temperature to clinically relevant values. Recently $Mn_{1-x}Ni_xFe_2O_4$ MNPs have been demonstrated being able to produce heat by irradiation with NIR light reaching temperatures suitable for application in hyperthermia-based therapies, without losing the capability to interact with an ac field opening the way for simultaneous magnetic-photo thermal therapy.

Espinosa *et al.* [24] showed that an adequate magneto-plasmonic design can efficiently combine photothermia with magnetic hyperthermia into an efficient bimodal thermo-therapy. The magneto-plasmonic nanohybrids were composed of an iron oxide core optimized for high efficiency in magnetic hyperthermia, and an Au shell with tunable plasmonic properties in the NIR region. They provided nanoscale characterization by mapping for the first time the plasmon around a magnetic oxide core, connecting unambiguously the optical response of single, isolated nanostructures with that of large assemblies. The system generated heat through a remarkable cumulative effect when both magnetic and plasmonic modalities were applied simultaneously and the heating efficiency was maintained *in vivo* conditions. The tumor temperature can then rapidly reach 48 °C for therapeutic tumor ablation with dose injected 10 times lower than that for classical magnetic hyperthermia treatment. Obviously, the refining of the synthetic technique in the production of hyperthermic nanostructures allows the realization of systems to overcome the limitations of both PTT and MHT.

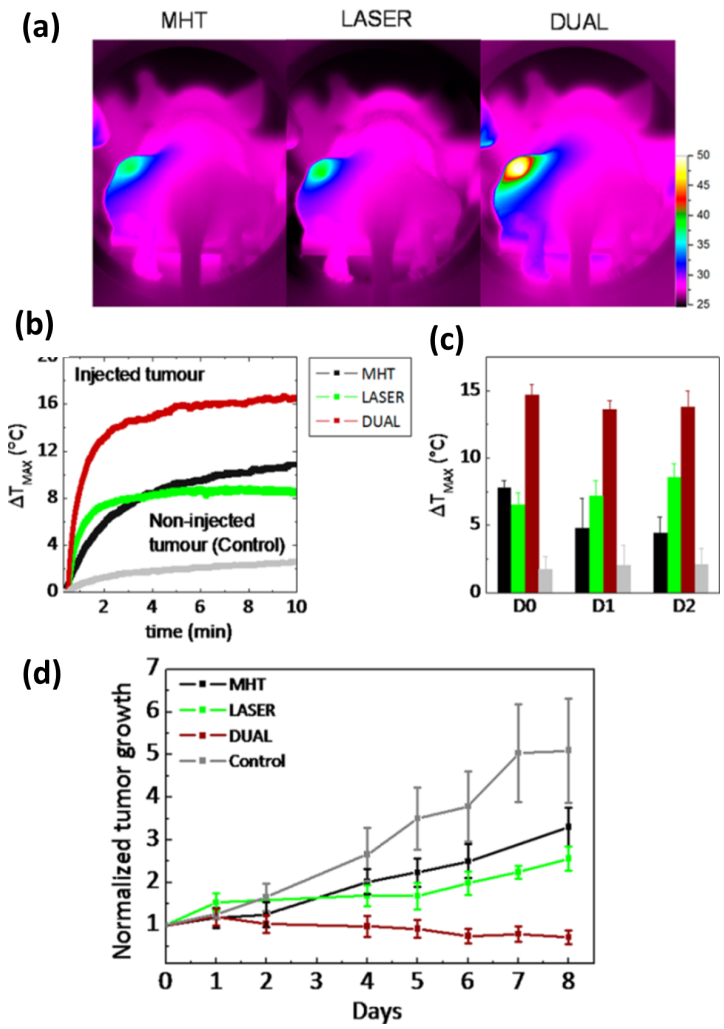


**Fig. 10:** *In vivo* heat therapy. a) Thermal images obtained with the IR camera in mice after intratumoral injection of nanocubes (50 µL at [Fe] = 250 mM), in the left-hand tumor, and after 10 min application of MHT (110 kHz, 12 mT), NIR-laser irradiation (LASER, 808 nm at 0.3 W/cm$^2$), or DUAL (both effects). b) Corresponding thermal elevation curves for all treatments and for the non-injected tumor in the DUAL condition. c) Average final temperature increase obtained after 10 min (MHT, LASER, and DUAL) on day 0 (1 h after injection) and 1 and 2 days after injection and for non-injected tumors. d) Average tumor growth (groups of six tumors each in non-injected mice submitted to no treatment (control) and in nanocube-injected mice exposed to MHT, LASER, and DUAL during the 8 days following the 3 days of treatment [14]. (Reprinted with permission from Ref. [13], Copyright 2016, American Chemical Society)

## 5. Prerequisites for hyperthermia treatment in the clinic

The methods and procedure for the production and functionalization of NPs for MHT and PTT have greatly improved in the last two decades, but these systems are still far from being ready for clinical uses. One of the obstacles for *in vivo* administration is the difficulty to measure and guarantee the stability of the material exposed to the complex conditions of the various biofluid and tissues present in a real body. Ideally, nanomaterials should be inert to the passage through the body, be able to accumulate in the cancerous tissue and quickly be eliminated (by excretion or digestion) by the host [31, 177]. The resistance of the nanomaterial to the physiological conditions and its interaction with the *in vivo* environment is broadly controlled by its surface modification and, on the protein corona, the nanomaterial form as soon it gets in contact with the biofluids (blood, lymphatic fluid, cerebral fluid or digestive fluids) [178, 179]. Another important parameter to control when adapting a nanomaterial to the clinical application is method of administration. Some nanomaterials with large size (*e. g.,* metallic Au or Ag NPs above ≈ 10 nm) can only be administered by injection or ingestion, while smaller ones or liposomes can be administered by aerosol or spray directly through the respiratory tract [180, 181].The method chosen to deliver the NPs to the tumor will define the limits of their behavior in the body. NPs without specific targeting will benefit from a long half-life in the blood stream (increasing the time available to exploit the higher permeability of the tumor tissue barrier) while if directly injected in a tumoral mass they will need to release the chemotherapic payload, or ablative hyperthermia and quickly be expelled from the body.

### 5.1. Parameter affecting toxicity: size, shape, composition, coating

The toxicity of PTT NPs depends on the type of material used for the formation of the particles and the substances for stabilization and targeting. Noble metal NPs are generally safe in biological condition while QDs, rare earth doped luminescent crystals and carbon nanostructures are toxic and a post-synthesis treatment is needed to make them safe in physiological conditions [182]. Toxicity of PTT NPs based on Au mostly depends on the presence of toxic residues left from the synthetic process (CTAB for nanorods, prism, cubes, cages and stars). Recent reviews showed reduced or no toxicity of Au NPs stabilized with polymers [183]. The size of the particles investigated also influence the level of toxicity and tests on mice show a reduction of the life expectancy of the animal when exposed to particles sized between 10- 40 nm [184].

A great number of studies have been conducted on the toxicity of IONPs in physiological condition [185], with results depending on the shape and the moieties present on its surface. In general, IONPs are not particularly toxic in physiological condition, but the toxicity becomes a factor with the presence of other elements Co, Cd, Mn and on the stability of the surface modification. For example, a surface passivate by iron hydroxide is relatively safe but if it is damaged by the contact with the biofluids it may trigger the production of toxic reactive oxygen species (ROS) [186]. For IONPs, coating with polymers or polysaccharides are usually preferred because of its low toxicity and minimal interaction with the host [187]. Studies using IONPs with proper stabilization have shown positive results in terms of safety for human patients [188].

Recent studies suggest that IONPs have no relevant toxicity for the concentrations used in the clinical treatments and there are guidelines available for the safe dosages and administration protocols [188]. At high concentrations, IONPs can be toxic if they accumulate around the

perinucleus of cells. The study with BLAB/c mice provided evidence of increased productions of enzymes in the liver treated with $Fe_3O_4$ NPs concentration of 150-300 µl/g below which the effect became limited [189]. On different shapes, most studies show no indication towards an effect of size on the biocompatibility except for the high toxicity observed in rod-shaped IONPs. It is noted that bare IONPs are toxic to the cells due to strong attractive electromagnetic interactions between the positive charge of the IONPs and the negative charge from the cell surface [185]. In the case of coating destruction or damage in the IONPs, toxicity can increase due to the precursors found in the synthesis of IONPs. Furthermore, physical stress and oxidative stress can also be induced in the cells as a result of their contact with naked IONPs.

**5.2. Biodistribution, pharmacokinetics and clearance rate**

Biodistribution and pharmacokinetics of IONPs incorporated into the host tend to be complicated [190]. IONPs which have been FDA approved are almost harmless to native organisms and sometime high concentrations can be used with limited side-effects. Recent studies have shown a size-dependent accumulation of IONPs in different organs in the body with the small size NPs found in the liver while the large ones travel to the spleen. Depending on where the IONPs are distributed, they are incorporated differently into the host, either on the hepatocytes where their degradation products transform into ferritin or on macrophages found in the spleen where they are degraded via phagocytosis [190]. Blood clearance rate seems to be proportional to hydrodynamic size rather than the choice of coating material [191] with a range of blood half-life observed to be from minutes to days [192,193].

The distribution and pharmaco-kinesis of PTT NPs are complex, and the scientific community has not reached a consensus on the matter, as for the toxicity, the retention time and the

activity of PTT depends from the size, material and coating of the particles. AuNPs having size below 15 nm stabilized with tiopronin or low weight PEG (2–4 kDa) introduced by intravenous injection are clear from the body in less than 25 h or 4–8 h, respectively. [194,195] Au NPs having size from 24 to 72 nm stabilized with long chain PEG (10 kDa) have a slower rate of clearance of 50 % in 7 days [184]. In the latter case, studies from Ali *et al.* [196] showed the presence of the particles in the kidney and spleen after 15 months from the injection without visible toxic effect on the mice. Small spherical Au NPs below 5 nm were reported to have some level of toxicity regardless of the composition or the stabilization [197]. According to the study of Nahle *et al.* [198] 50 % of the amount of multi-walled carbon nanotubes injected to a mice get eliminated in the first 24 h, the remaining can still be found in the lungs, liver and spleen after 28 days from the injection. QD based PTT NPs remains in the circulatory system up to 72 h with half of the particles getting cleared in the first 8 h after the injection [155].

**5.3. Concentration required for treatment**

There is no consensus on the specific amount of NPs (mg/kg) to be used to generate the hyperthermal effect, mostly because the efficiency, the delivery system and the level of heating can vary wildly between the different variety of HT. Paul Southern *et al.* [199], have identified a range of 2.5 mg/kg to 8.5 mg/kg as dose range for the use of commercially available superparamagnetic NPs in hyperthermia and indicated a series of parameters and variables to consider when defining the posology for new types of particles. While Espinosa *et al.* [200] in their comparative study with different nanostructures for PTT and MHT have identified an increase of the efficiency linear with the concentration tested (0.25; 2.5 or 25 mg/kg) for MHT while NPs for PTT seems reach an higher efficiency when administer at lower concentrations

(0.25 mg/kg for nanocubes or rods). Studies in mice with IONPs at concentrations of 250 µg/mL (150 µl) [53] and 14 mg/mL (50 µL) [201] were reported. No significant toxicity was observed in these studies, while IONPs seemed to clear out from the body rapidly (approximately 24 h as reported from Wang *et al.* [145]). The majority of the studies on *in vivo* photo-activated hyperthermia or biodistribution [184] used 100 µL of 10 mg/mL NPs solution, for Au based particles. Early studies from Dickerson *et al.* [202] used direct injection of 10 µL (OD800= 200) particles solution in the tumoral mass. Ding *et al.* [203] used 50 µL of 2 mg/mL solution to obtain the thermal ablation of breast cancer grafted on nude mice. QDs CdSe-ZnS particles have shown activity for a quantity of 20 µL of 2 mg/mL dispersion as seen in the study of Yong *et al* 2015.The concentration of particles used for PTT depends on the type and depth of tumors. However, since the studies were on immunodeficient mice, the findings might not provide a solid foundation for evaluating the safe concentration to be used in animals when treated with PTT and MHT.

**5.4. Drug release by external thermal therapy**

Hyperthermia cancer treatments using magnetic and photothermal methods are still facing many challenges due to non-uniform thermal profile within the tumor, the lack of knowledge of the molecular mechanisms involved in the cellular damage, the reservation from the medical community and the difficulties to access the technical facilities needed for the treatment. Recent researches suggested more fruitful results using hyperthermia accompanying with drug or therapeutic molecules attached on the surface of NPs. In parallel of heat generation due to magnetic field or photothermal effect to induce cell death, the temperature increase can trigger the release or the activation of therapeutic molecules. Here it is valuable to understand

the release of such drug molecules sensitive to external stimuli such as temperature, pH, enzymatic conditions, etc. The use of temperature (an external stimulus) affecting the drug release could be more relevant as it is controllable exactly where and when a drug payload is released. The approach has been widely explored, using stimuli such as light (photothermal) and magnetic hyperthermia. The advantages of external stimuli of drug release include: (i) the therapeutic molecules are protected from premature degradation in the body before reaching the targeted area, and (ii) it allows the better control of the active timing at the desired time point.

Usually, a thermo-responsive polymer or liposome matrix is coated over NPs to release antitumoral agents or drugs, mediated by hyperthermia actions. A few methodologies have been employed to realize temperature dependent drug release [204–206]: (i) by breaking or destabilization of the bond between the therapeutic molecule and the matrix, allowing its release; (ii) by the advantage of the heat-induced transformation of the thermo-responsive matrix, allowing the escape of the therapeutic drug from the matrix, mainly based on the use of thermo-responsive polymers or magneto-liposomes; (iii) use of a porous material, where the therapeutic agents are retained, whose pores (called as switchable gates) are blocked by a thermo-responsive material; and (iv) degradation of the matrix, allowing the release of its cargo, using thermo-sensitive polymers that undergo a dissolution process at higher temperatures. Drugs could be carried out by several possible ways such as polymer based NPs, magneto-liposomes, micelles, ferrogels, Au-MNPs (Au@MNPs), mesoporous silica-MNPs (mSi@MNPs) etc.

The magnetic hyperthermia as external stimuli present several additional advantages. Using field gradients from Magnetic Particle Imaging (MPI) equipment, it is possible to control the spatial localization of the release of therapeutic molecules, which avoids problems related to side effects and systemic cytotoxicity.

Bear *et al.* [207] studied magnetic hyperthermia controlled drug release in gastrointestinal (GI) tract based on coating standard gelatin drug capsules with a model eicosane- SPIONPs composite, which is activated using magnetic hyperthermia as an on demand release mechanism to heat and melt the coating [207]. Rose *et al* presented an iron oxide nanoparticle/wax composite capsule coating that protects the capsule contents from the highly variable chemical conditions of the GI tract [208]. It can be triggered using magnetic hyperthermia initiated from an external *ac* magnetic field. The coating was produced from pharmaceutically approved materials and was applied using a simple dip-coating process utilizing a gelatin drug capsule as a template.

A SPION carrier encapsulated within a cross-linked polyethylene/propylene oxide polymer shell capsule (containing vitamin B12 as a model drug) showed fluctuations by swelling and contracting as a response of change in temperature [209]. With conventional heating to 45 °C, the core-shell structure was observed to contract causing extrusion of the therapeutic cargo and leaching 40 % of the full payload in the first 5 min. Rapid on-demand release at the target site is then possible with brief application of an external *ac* magnetic field, thus limiting off target effects of the drug. Caetano and others studied magnetic hyperthermia-induced drug release nanocomposites by conjugation of ureasil cross-linked poly(ethylene oxide) hybrid materials from U-PEO-γ-$Fe_2O_3$ [210].

Likewise, temperature raised due to magnetic hyperthermia, near infrared laser are useful to increase the temperature through photothermal effect and several examples have been provided with the requirements of good photothermal agent as good biocompatibility, photothermal conversion efficacy and stability. In order to improve the tumor inhibition ability, anti-tumor drugs are usually loaded on photothermal agents to fabricate drug-loaded system. The raised temperature can accelerate drug delivery rate due to the improved molecular movement rate. Thus, drug-loaded photothermal agent can exert chemo-photothermal synergetic therapy effect to tumor inhibition. Zhang *et al* used amino-terminated hyperbranched polymer (HBP) to prepare hydrophilic rGO conjugated with doxorubicin hydrochloride (DOX) as a drug loading system, and probed photothermal abilities as well as a pH/photothermal dual-responsive drug delivery behavior [80]. At acidic environment or under NIR laser irradiation, the drug release rate could be improved, which is beneficial to control release anti-tumor drug in tumor tissues.

In a study performed by Shen *et al*. [211], DOX encapsulated (90.9 % efficiency) MNPs-loaded thermosensitive liposomes (DOX-$Fe_3O_4$–TSL) utilized NIR laser-triggered release and combined photothermal–chemotherapy of tumors, significantly improved drug release compared to that of DOX–TSL. Recently, Wu *et al.* reported a novel photothermally controlled intelligent drug release system (AuNP@m$SiO_2$-DOX-FA) with a large amount of drugs loading for synergistic chemo-photothermal therapy of MDR in breast cancer [212]. The nanoplatform utilized Au NPs as a hyperthermia core, and large-mesoporous silica as a shell for DOX loading [212, 213]. Benefiting from the thick layer and large pore size, the encapsulation and loading efficiency were as high as 97.7 % and 8.84 %, respectively.

### 5.5.*In vivo* and clinical application of hyperthermia treatments

#### 5.5.1. Tumor microenvironment and hyperthermia effects

Shifting the experimental conditions from *in vitro* testing to *in vivo* applications introduce a new layer of complexity to the use of hyperthermia treatments. When a tumor mass grow enough to became a solid tumor or in presence of pre metastatic niches [214] it generates a peculiar tumor microenvironments (TME), which could limit the efficiency of traditional anticancer treatment or interfere with the mechanism of action of drugs [215]. A tumor has in average a more acidic pH compared to healthy tissue and when it reaches a certain mass it will progressively loose vascularization which slow down the general growth of the tumor but also reduce the efficiency of traditional drugs [205]. At the same time these condition trigger a cascade of complex metabolic pathways and the activation of proteins, both in the tumour than in the surrounding cells, which have to be understood to improve the efficiency of hyperthermia treatments [216, 217]. Recent studies have pointed out the importance of the changes that PHT infer to the TME. The hyperthermal process stimulates the restoration of the vascularization of the tumor area, while modifying the extracellular media condition. These changes increases the effectivity of anticancer drugs and exposes the tumor to the action of the body immune system [218]. For MH the high tunability of the heating process of MNPs has been used to trigger specific changes in the TME in order to increase the tumor vulnerability to the anticancer procedure [219].

#### 5.5.2. Delivery routes of nanoparticles in tumors

One of the challenges of developing *in vivo* applications for hyperthermia NPs is the capability to deliver a suitable amount of NPs to the tumor region to be able to generate a strong hyperthermal effect. The delivery issue is common to all types of particles, but it is mitigated by the characteristic of tumor cells to be easier penetrated by NPs than healthy cells, while being less vascularized and more corrugated tend to retain particles for longer time, thus the definition of enhanced penetration/retention (EPR) of tumors. Numerous studies had been focused in pointing out the NPs parameters which maximize the EPR effect [204, 220, 221], while other followed a more active targeting philosophy working on modifying the surface of particles with specific antigens or molecules able to interact with specific tumors [222–224].

**5.5.3. Examples of in vivo and clinical application of hyperthermia treatment**

Over the last decade, there have been a great number of studies on the effect of hyperthermia on mice or other small animals as can be seen from the data previously reported on the biodistribution and toxicity of the nanomaterials used for hyperthermia [225, 226], with good results in eliminating the cancer tissue and in increasing the survivability of test mice [4, 227–229]. But the number of approved nanodrugs for clinical trials is still very limited. Nanotherm® a SPION based nanomedicine, for the treatment of breast cancer in the lymph-nodal system, has been recently approved for clinical use by the EU and it is passing the final stages of approval by the FDA [230]. Other nanomaterial based nanomedicine for hyperthermia have been approved by the FDA for clinical trials with mixed results (Feraheme®, Ferumoxytol [231] and Feridex® [232]) all based on SPION coated with polysaccharides. While in the field of the PTT only Aurolase and AuroLase Treatment (for the ablation of prostate cancer tissue) a medical device

based on Au nanoshells have been approved for a series of pilots clinical trials for head and neck tumors, lung and prostate cancer [233].

**6. Conclusion and future perspectives**

To summarize, we have reviewed a detail of thermal treatments and their diverse applications. The aim of thermal treatment using nanoscaled materials is the ablation of tumor and killing of cancer cells. A description and mechanism of MHT and various spectroscopic mechanism of PTT has been provided together in this review. Recent examples from clinical trials has been taken to explain the importance of the topic and under clinical trial nanomaterials. Technical information regarding instrumentation is also provided for the readers. A detailed example of magnetic materials, QDs, lanthanides, carbon based materials, plasmonic materials has been reviewed and process of heat generation is explained. Further, since both therapies have their own intrinsic limitations, we surveyed literature over a combined thermal therapy which is still at its infancy state. We strongly advocate this kind of approach through designing new anisotropically grown multifunctional nanohybrids.

Multifunctional hybrid-design nanomaterials appear to be promising to meet current therapeutics for efficient cancer treatment. Herein, two efficient heat nanogenerators were combined into a multifunctional single nanohybrid (a multi-core IONPs optimized for magnetic hyperthermia, and an Au or lanthanides branched shell/satellite with tunable plasmonic properties in the NIR region, for photothermal therapy) which impressively enhanced heat generation, in suspension or in tumors, opening up exciting new therapeutic perspectives. It is equally important to develop new methodology and mechanism of light to tissue heat transfer.

Such developments may require new multimodal experimental setups to understand complex behavior of NP heating, tracking, sensing, delivery simultaneously.

The realistic approach for the design of magnetic NPs should have the highest possible specific loss power (SLP), i.e. ILP, under biological constraints in SPM regime, by tuning anisotropic energy through core-shell or alloying hard-soft ferrites in small tumors and metastases. Photothermal therapy usually comprises low power 808 nm laser through ultrasmall optical nanomaterials. The biggest challenge in thermal nanomedicine is the real time information about intra-tumoral temperature (microscopic). Thermal camera has been widely used or optical fiber (a non-invasive) technique are being used to know temperatures. Both the techniques have problems. Here through this review article, we hope to open up many avenues for combined photo-magnetic thermal therapy with non-invasive temperature feedback.

**Conflict of interest:** There are no conflicts of interest to declare.

**Acknowledgement:** FR & NTKT thanks EPSRC (EP/M018016/1) for funding, LDT, FR & NTKT thanks AOARD grant (FA2386-17-1-4042 ) for funding. SKS thanks to PPPGI-UFMA, PPGF-UFMA and FAPEMA, Brazil for financial support. NS thanks to CNPq, Brazil for the post-doctoral fellowship (PDJ 152208/2018-6). The authors thank Sarveena and Nina Christou for insightful discussion.

**References:**


[1] S. Sotoma, C.P. Epperla, H.-C. Chang, ChemNanoMat, 1, (2018), pp. 15–27.
[2] G. Kucsko, P.C. Maurer, N.Y. Yao, M. Kubo, H.J. Noh, P.K. Lo, et al., Nature, 7460, (2013), pp. 54–58.
[3] A. Szasz, O. Szasz, N. Szasz, in: Hyperth. Cancer Treat. A Prim., Springer US, Boston, MA, n.d., pp. 27–59.
[4] A.E. Dunn, D.J. Dunn, M. Lim, C. Boyer, N.T.K. Thanh, in: Nanosci. 2, 2013, pp. 225–254.
[5] R.W.Y. Habash, R. Bansal, D. Krewski, H.T. Alhafid, Critical reviews in biomedical engineering, 6, (2006), pp. 459–89.
[6] D. Jaque, L. Martínez Maestro, B. del Rosal, P. Haro-Gonzalez, A. Benayas, J.L. Plaza, et al., Nanoscale, 16, (2014), pp. 9494–9530.
[7] Z. Behrouzkia, Z. Joveini, B. Keshavarzi, N. Eyvazzadeh, R.Z. Aghdam, Oman medical journal, 2, (2016), pp. 89–97.
[8] S. Jha, P.K. Sharma, R. Malviya, Achievements in the Life Sciences, 2, (2016), pp. 161–167.
[9] P. Chakravarty, R. Marches, N.S. Zimmerman, A.D.-E. Swafford, P. Bajaj, I.H. Musselman, et al., Proceedings of the National Academy of Sciences, 25, (2008), pp. 8697–8702.
[10] M. Drakopoulou, C. Moldovan, K. Toutouzas, Current Opinion in Pharmacology, (2018), pp. 99–104.
[11] A. LeBrun, R. Ma, L. Zhu, Journal of Thermal Biology, Pt B, (2016), pp. 129–137.
[12] A. Hervault, N.T.K. Thanh, Nanoscale, 20, (2014), pp. 11553–11573.
[13] S. Jha, P.K. Sharma, R. Malviya, Achievements in the Life Sciences, 2, (2016), pp. 161–167.
[14] A. Espinosa, R. Di Corato, J. Kolosnjaj-Tabi, P. Flaud, T. Pellegrino, C. Wilhelm, ACS Nano, 2, (2016), pp. 2436–2446.
[15] S.R. Grobmyer, N. Iwakuma, P. Sharma, B.M. Moudgil, in: 2010, pp. 1–9.
[16] A. Singh, S.K. Sahoo, Drug Discovery Today, 4, (2014), pp. 474–481.
[17] E. Blanco, H. Shen, M. Ferrari, Nature Biotechnology, 9, (2015), pp. 941–951.
[18] D. Jaque, L. Martínez Maestro, B. del Rosal, P. Haro-Gonzalez, A. Benayas, J.L. Plaza, et al., Nanoscale, 16, (2014), pp. 9494–9530.
[19] A. Sharma, A.K. Goyal, G. Rath, Journal of Drug Targeting, 8, (2018), pp. 617–632.
[20] R.A. Revia, M. Zhang, Materials Today, 3, (2016), pp. 157–168.
[21] N. Lee, D. Yoo, D. Ling, M.H. Cho, T. Hyeon, J. Cheon, Chemical Reviews, 19, (2015), pp. 10637–10689.
[22] A. Jordan, K. Maier-Hauff, Journal of nanoscience and nanotechnology, 12, (2007), pp. 4604–6.
[23] A.B. Salunkhe, V.M. Khot, S.H. Pawar, Current topics in medicinal chemistry, 5, (2014), pp. 572–94.
[24] A. Espinosa, M. Bugnet, G. Radtke, S. Neveu, G.A. Botton, C. Wilhelm, et al., Nanoscale, 45, (2015), pp. 18872–18877.
[25] E.C. Dreaden, A.M. Alkilany, X. Huang, C.J. Murphy, M.A. El-Sayed, Chemical Society reviews, 7, (2012), pp. 2740–79.
[26] Z. Zhang, J. Wang, C. Chen, Theranostics, 3, (2013), pp. 223–238.
[27] Z.-C. Wu, W.-P. Li, C.-H. Luo, C.-H. Su, C.-S. Yeh, Advanced Functional Materials, 41, (2015), pp. 6527–6537.

[28] Z. Zhang, J. Wang, X. Nie, T. Wen, Y. Ji, X. Wu, et al., Journal of the American Chemical Society, 20, (2014), pp. 7317–7326.
[29] A.N. Bashkatov, E.A. Genina, V.I. Kochubey, V. V Tuchin, Journal of Physics D: Applied Physics, 15, (2005), pp. 2543–2555.
[30] E. Myrovali, N. Maniotis, A. Makridis, A. Terzopoulou, V. Ntomprougkidis, K. Simeonidis, et al., Scientific reports, (2016), pp. 37934.
[31] C.L. Ventola, Pharmacy and Therapeutics, 12, (2017), pp. 742.
[32] D. Ortega, Q.A. Pankhurst, in Nanoscience: Volume 1: Nanostructures through Chemistry, P. O'Brien, Editor. 2013, Royal Society of Chemistry, Cambridge, (2012), pp. 60–88.
[33] E.A. Périgo, G. Hemery, O. Sandre, D. Ortega, E. Garaio, F. Plazaola, et al., Applied Physics Reviews, 4, (2015), pp. 041302.
[34] S. Dutz, R. Hergt, International Journal of Hyperthermia, 8, (2013), pp. 790–800.
[35] R.K. GILCHRIST, R. MEDAL, W.D. SHOREY, R.C. HANSELMAN, J.C. PARROTT, C.B. TAYLOR, Annals of surgery, 4, (1957), pp. 596–606.
[36] M. Osaci, M. Cacciola, IOP Conference Series: Materials Science and Engineering, 1, (2017), pp. 012008.
[37] M.S. Carrião, A.F. Bakuzis, Nanoscale, 15, (2016), pp. 8363–8377.
[38] I. Hilger, International Journal of Hyperthermia, 8, (2013), pp. 828–834.
[39] R.R. Wildeboer, P. Southern, Q.A. Pankhurst, Journal of Physics D: Applied Physics, 49, (2014), pp. 495003.
[40] R. Hergt, S. Dutz, R. Müller, M. Zeisberger, Journal of Physics: Condensed Matter, 38, (2006), pp. S2919–S2934.
[41] D. Ortega, Q.A. Pankhurst, in: 2012, pp. 60–88.
[42] E. Esmaeili, R.G. Chaydareh, S. Farsad, S.A. Rounaghi, N. Mollayi, Chemical Engineering Communications, 9, (2016), pp. 1157–1164.
[43] R. Hergt, S. Dutz, M. Zeisberger, Nanotechnology, 1, (2010), pp. 015706.
[44] S. Laurent, S. Dutz, U.O. Häfeli, M. Mahmoudi, Advances in Colloid and Interface Science, 1–2, (2011), pp. 8–23.
[45] G. Glöckl, R. Hergt, M. Zeisberger, S. Dutz, S. Nagel, W. Weitschies, Journal of Physics: Condensed Matter, 38, (2006), pp. S2935–S2949.
[46] V.N. Nikiforov, Russian Physics Journal, 9, (2007), pp. 913–924.
[47] R. Hergt, S. Dutz, Journal of Magnetism and Magnetic Materials, 1, (2007), pp. 187–192.
[48] P. Guardia, R. Di Corato, L. Lartigue, C. Wilhelm, A. Espinosa, M. Garcia-Hernandez, et al., ACS Nano, 4, (2012), pp. 3080–3091.
[49] R.R. Shah, T.P. Davis, A.L. Glover, D.E. Nikles, C.S. Brazel, Journal of Magnetism and Magnetic Materials, (2015), pp. 96–106.
[50] R.E. Rosensweig, Journal of Magnetism and Magnetic Materials, (2002), pp. 370–374.
[51] K.M. Krishnan, IEEE transactions on magnetics, 7, (2010), pp. 2523–2558.
[52] A.E. Deatsch, B.A. Evans, Journal of Magnetism and Magnetic Materials, (2014), pp. 163–172.
[53] I. Obaidat, B. Issa, Y. Haik, Nanomaterials, 4, (2015), pp. 63–89.
[54] M. Harabech, J. Leliaert, A. Coene, G. Crevecoeur, D. Van Roost, L. Dupré, Journal of Magnetism and Magnetic Materials, (2017), pp. 206–210.
[55] N. Knežević, I. Gadjanski, J.O. Durand, J. Mater. Chem. B 7, (2019), pp.9–23.

[56] C.S.S.R. Kumar, F. Mohammad, Advanced Drug Delivery Reviews, 9, (2011), pp. 789–808.
[57] W.S. Seo, J.H. Lee, X. Sun, Y. Suzuki, D. Mann, Z. Liu, et al., Nature Materials, 12, (2006), pp. 971–976.
[58] C. Wang, S. Peng, L.M. Lacroix, S. Sun, Nano Research, 5, (2009), pp. 380–385.
[59] P. Tartaj, T. González-Carreño, C.J. Serna, Advanced Materials, 21, (2001), pp. 1620–1624.
[60] M.H. Falk, R.D. Issels, International journal of hyperthermia : the official journal of European Society for Hyperthermic Oncology, North American Hyperthermia Group, 1, (n.d.), pp. 1–18.
[61] P.H. Linh, N.X. Phuc, L. V. Hong, L.L. Uyen, N. V. Chien, P.H. Nam, et al., Journal of Magnetism and Magnetic Materials, (2018), pp. 128–136.
[62] R.M. Patil, N.D. Thorat, P.B. Shete, P.A. Bedge, S. Gavde, M.G. Joshi, et al., Biochem. Biophys. Reports 13, (2018), pp.63–72.
[63] S. Del Sol-Fernández, Y. Portilla-Tundidor, L. Gutiérrez, O.F. Odio, E. Reguera, D.F. Barber, et al., ACS Applied Materials & Interfaces, 30, (2019), pp. 26648–26663.
[64] E.L. Verde, G.T. Landi, J.A. Gomes, M.H. Sousa, A.F. Bakuzis, Journal of Applied Physics, 12, (2012), pp. 123902.
[65] C.L. Dennis, R. Ivkov, International Journal of Hyperthermia, 8, (2013), pp. 715–729.
[66] D.-H. Kim, E.A. Rozhkova, I. V. Ulasov, S.D. Bader, T. Rajh, M.S. Lesniak, et al., Nature Materials, 2, (2010), pp. 165–171.
[67] Z. Nemati, S.M. Salili, J. Alonso, A. Ataie, R. Das, M.H. Phan, et al., Journal of Alloys and Compounds, (2017), pp. 709–714.
[68] S.A. Mark Griswold, L.M. Bauer, S.F. Situ, M.A. Griswold, A.S. Cristina Samia, Nanoscale, (2016), pp. 12162–12169.
[69] R. Das, J. Alonso, Z. Nemati Porshokouh, V. Kalappattil, D. Torres, M.-H. Phan, et al., The Journal of Physical Chemistry C, 18, (2016), pp. 10086–10093.
[70] Z. Nemati, J. Alonso, L.M. Martinez, H. Khurshid, E. Garaio, J.A. Garcia, et al., The Journal of Physical Chemistry C, 15, (2016), pp. 8370–8379.
[71] P. Pradhan, J. Giri, G. Samanta, H.D. Sarma, K.P. Mishra, J. Bellare, et al., Journal of Biomedical Materials Research Part B: Applied Biomaterials, 1, (2007), pp. 12–22.
[72] E.C. Abenojar, S. Wickramasinghe, J. Bas-Concepcion, A.C.S. Samia, Progress in Natural Science: Materials International, 5, (2016), pp. 440–448.
[73] G.T. Landi, Physical Review B, 1, (2014), pp. 014403.
[74] J. Carrey, B. Mehdaoui, M. Respaud, Journal of Applied Physics, 8, (2011), pp. 083921.
[75] R.P. Tan, J. Carrey, M. Respaud, Physical Review B, 21, (2014), pp. 214421.
[76] Y. Chalopin, J.-C. Bacri, F. Gazeau, M. Devaud, Scientific Reports, 1, (2017), pp. 1656.
[77] Z. Sabsabi, F. Vernay, O. Iglesias, H. Kachkachi, Physical Review B, 10, (2013), pp. 104424.
[78] M. Knobel, W.C. Nunes, L.M. Socolovsky, E. De Biasi, J.M. Vargas, J.C. Denardin, Journal of Nanoscience and Nanotechnology, 6, (2008), pp. 2836–2857.
[79] M. Wuithschick, A. Birnbaum, S. Witte, M. Sztucki, U. Vainio, N. Pinna, et al., ACS Nano, 7, (2015), pp. 7052–7071.
[80] W. Zhang, J. Dai, G. Zhang, Y. Zhang, S. Li, D. Nie, Nanoscale Research Letters, (2018),.
[81] C. Blanco-Andujar, D. Ortega, P. Southern, Q.A. Pankhurst, N.T.K. Thanh, Nanoscale, 5, (2015), pp. 1768–1775.

[82] K. Brooks, J. Yatvin, C.D. McNitt, R.A. Reese, C. Jung, V. V. Popik, et al., Langmuir, 26, (2016), pp. 6600–6605.
[83] M. Jeun, S. Bae, A. Tomitaka, Y. Takemura, K.H. Park, S.H. Paek, et al., Applied Physics Letters, 8, (2009), pp. 082501.
[84] M. Suto, Y. Hirota, H. Mamiya, A. Fujita, R. Kasuya, K. Tohji, et al., Journal of Magnetism and Magnetic Materials, 10, (2009), pp. 1493–1496.
[85] A.G. Roca, B. Wiese, J. Timmis, G. Vallejo-Fernandez, K. O'Grady, IEEE Transactions on Magnetics, 11, (2012), pp. 4054–4057.
[86] J.-P. Fortin, C. Wilhelm, J. Servais, C. Ménager, J.-C. Bacri, F. Gazeau, JACS, 9, (2007), pp. 2628–2635.
[87] W.-K. Fong, T.L. Moore, S. Balog, D. Vanhecke, L. Rodriguez-Lorenzo, B. Rothen-Rutishauser, et al., in: Springer, Cham, 2019, pp. 101–150.
[88] H. Köçkar, O. Karaagac, F. Özel, Journal of Magnetism and Magnetic Materials, (2019), pp. 332–336.
[89] I. Robinson, N.T.K. Thanh, International Journal of Nanoscience, 4&5, (2011), pp. 883–890.
[90] C. Blanco-Andujar, L.D. Tung, N.T.K. Thanh, Annual Reports Section "A" (Inorganic Chemistry), 0, (2010), pp. 553.
[91] Thanh Nguyen T K, I. Robinson, L.D. Tung, Dekker Encyclopedia of Nanoscience and Nanotechnology, 1, (2007), pp. 1–10.
[92] R.M. Pallares, X. Su, S.H. Lim, N.T.K. Thanh, Journal of Materials Chemistry C, 1, (2016), pp. 53–61.
[93] C. Blanco-Andujar, D. Ortega, Q.A. Pankhurst, N.T.K. Thanh, Journal of Materials Chemistry, 25, (2012), pp. 12498–12506.
[94] S. Tong, C.A. Quinto, L. Zhang, P. Mohindra, G. Bao, ACS Nano, 7, (2017), pp. 6808–6816.
[95] A. Hervault, A.E. Dunn, M. Lim, C. Boyer, D. Mott, S. Maenosono, et al., Nanoscale, 24, (2016), pp. 12152–61.
[96] C.L. Dennis, A.J. Jackson, J.A. Borchers, R. Ivkov, A.R. Foreman, P.J. Hoopes, et al., Journal of Physics D: Applied Physics, 13, (2008), pp. 134020.
[97] W. Zhang, C. Wu, S.R.P. Silva, Expert Review of Anticancer Therapy, 8, (2018), pp. 723–725.
[98] V. Mameli, A. Musinu, A. Ardu, G. Ennas, D. Peddis, D. Niznansky, et al., Nanoscale, 19, (2016), pp. 10124–10137.
[99] S. Balasubramanian, A. Ravindran Girija, Y. Nagaoka, T. Fukuda, S. Iwai, V. Kizhikkilot, et al., RSC Advances, 32, (2015), pp. 25066–25078.
[100] A.-T. Le, C.D. Giang, L.T. Tam, T.Q. Tuan, V.N. Phan, J. Alonso, et al., Nanotechnology, 15, (2016), pp. 155707.
[101] C. Niu, Z. Wang, G. Lu, T.M. Krupka, Y. Sun, Y. You, et al., Biomaterials, 9, (2013), pp. 2307–2317.
[102] S. Noh, S.H. Moon, T.-H. Shin, Y. Lim, J. Cheon, Nano Today, (2017), pp. 61–76.
[103] S. Famiani, A.P. LaGrow, M.O. Besenhard, S. Maenosono, N.T.K. Thanh, Chemistry of Materials, 24, (2018), pp. 8897–8904.
[104] K.C.-F. Leung, S. Xuan, X. Zhu, D. Wang, C.-P. Chak, S.-F. Lee, et al., Chem. Soc. Rev., 5, (2012), pp. 1911–1928.

[105] Q. Zhang, I. Castellanos-Rubio, R. Munshi, I. Orue, B. Pelaz, K.I. Gries, et al., Chemistry of Materials, 21, (2015), pp. 7380–7387.
[106] J.-H. Lee, J. Jang, J. Choi, S.H. Moon, S. Noh, J. Kim, et al., Nature Nanotechnology, 7, (2011), pp. 418–422.
[107] S. He, H. Zhang, Y. Liu, F. Sun, X. Yu, X. Li, et al., Small, 29, (2018), pp. 1800135.
[108] M. Ma, Y. Wu, J. Zhou, Y. Sun, Y. Zhang, N. Gu, Journal of Magnetism and Magnetic Materials, 1–2, (2004), pp. 33–39.
[109] M.E. Sadat, R. Patel, J. Sookoor, S.L. Bud'ko, R.C. Ewing, J. Zhang, et al., Materials Science and Engineering: C, (2014), pp. 52–63.
[110] M. Kallumadil, Towards a Complete Magnetic Hyperthermia Technology as a Novel Cancer Treatment System, PhD Thesis, UCL (University College London), 2011.
[111] L.A. Thomas, Nanoparticle Synthesis for Magnetic Hyperthermia, PhD Thesis, UCL (Univeristy College London), (2010).
[112] C. Blanco-Andujar, D. Ortega, P. Southern, S.A. Nesbitt, N.T.K. Thanh, Q.A. Pankhurst, Nanomedicine, 2, (2016), pp. 121–136.
[113] J. Oh, H. Yoon, J.-H. Park, Biomedical Engineering Letters, 2, (2013), pp. 67–73.
[114] S.K. Ghosh, T. Pal, Chemical Reviews, 11, (2007), pp. 4797–4862.
[115] P.K. Jain, X. Huang, I.H. El-Sayed, M.A. El-Sayed, Plasmonics, 3, (2007), pp. 107–118.
[116] R.M. Pallares, X. Su, S.H. Lim, N.T.K. Thanh, Journal of Materials Chemistry C, 1, (2016), pp. 53–61.
[117] R. Robinson, W. Gerlach, H. Ghandehari, Journal of Controlled Release, (2015), pp. 245–252.
[118] G. Mie, Annalen der Physik, 3, (1908), pp. 377–445.
[119] M.A. Yurkin, A.G. Hoekstra, Journal of Quantitative Spectroscopy and Radiative Transfer, (2007), pp. 558–589.
[120] F. Gong, Z. Hongyan, D. V Papavassiliou, K. Bui, C. Lim, H.M. Duong, Nanotechnology, 20, (2014), pp. 205101.
[121] R. Singh, S. V. Torti, Advanced Drug Delivery Reviews, 15, (2013), pp. 2045–2060.
[122] G. Zhang, B. Li, The Journal of chemical physics, 11, (2005), pp. 114714.
[123] M.E. Sadat, M. Kaveh Baghbador, A.W. Dunn, H.P. Wagner, R.C. Ewing, J. Zhang, et al., Applied Physics Letters, 9, (2014), pp. 091903.
[124] C. Nerine J., L. Dorion B., L. Jennifer A., D. Hongmei, Z. Jin Z., J of Phys. Chem. B., 5, (1998), pp. 770–776.
[125] Z. Zhang, J. Wang, C. Chen, Advanced Materials, 28, (2013), pp. 3869–3880.
[126] Z. Qin, Y. Wang, J. Randrianalisoa, V. Raeesi, W.C.W. Chan, W. Lipiński, et al., Scientific Reports, 1, (2016), pp. 29836.
[127] J. Liu, C. Wang, X. Wang, X. Wang, L. Cheng, Y. Li, et al., Advanced Functional Materials, 3, (2015), pp. 384–392.
[128] R. Pązik, E. Zachanowicz, B. Pożniak, M. Małecka, A. Zięcina, Ł. Marciniak, RSC Adv., 29, (2017), pp. 18162–18171.
[129] W. Zhou, X. Liu, J. Ji, Journal of Nanoparticle Research, 9, (2012), pp. 1128.
[130] Y. Wang, K. Wang, J. Zhao, X. Liu, J. Bu, X. Yan, et al., Journal of the American Chemical Society, 12, (2013), pp. 4799–4804.
[131] S. Ghosh, S. Dutta, E. Gomes, D. Carroll, R. D'Agostino, J. Olson, et al., ACS Nano, 9,

(2009), pp. 2667–2673.
[132] M. Ema, M. Gamo, K. Honda, Regulatory Toxicology and Pharmacology, (2016), pp. 42–63.
[133] C. Cheng, K.H. Müller, K.K.K. Koziol, J.N. Skepper, P.A. Midgley, M.E. Welland, et al., Biomaterials, 25, (2009), pp. 4152–4160.
[134] V. Krishna, A. Singh, P. Sharma, N. Iwakuma, Q. Wang, Q. Zhang, et al., Small, 20, (2010), pp. 2236–2241.
[135] L. Cheng, C. Wang, L. Feng, K. Yang, Z. Liu, Chemical Reviews, 21, (2014), pp. 10869–10939.
[136] S.S. Lucky, K.C. Soo, Y. Zhang, Chemical Reviews, 4, (2015), pp. 1990–2042.
[137] B. Khlebtsov, V. Zharov, A. Melnikov, V. Tuchin, N. Khlebtsov, Nanotechnology, 20, (2006), pp. 5167–5179.
[138] B. Nikoobakht, M.A. El-Sayed, Chemistry of Materials, 10, (2003), pp. 1957–1962.
[139] L. Tong, Y. Zhao, T.B. Huff, M.N. Hansen, A. Wei, J.-X. Cheng, Advanced Materials, 20, (2007), pp. 3136–3141.
[140] J. Chen, B. Wiley, Z.-Y. Li, D. Campbell, F. Saeki, H. Cang, et al., Advanced Materials, 18, (2005), pp. 2255–2261.
[141] D.P. O'Neal, L.R. Hirsch, N.J. Halas, J.D. Payne, J.L. West, Cancer Letters, 2, (2004), pp. 171–176.
[142] H. Yuan, C.G. Khoury, H. Hwang, C.M. Wilson, G.A. Grant, T. Vo-Dinh, Nanotechnology, 7, (2012), pp. 75102–75111.
[143] Gang Yuan, Yongjie Yuan, Kan Xu, and, Qi Luo, Int. J. Mol. Sci., (2014), pp. 18776–18788.
[144] M. Chu, Y. Shao, J. Peng, X. Dai, H. Li, Q. Wu, et al., Biomaterials, 16, (2013), pp. 4078–4088.
[145] J. Wang, H. Zhao, Z. Zhou, P. Zhou, Y. Yan, M. Wang, et al., ACS Applied Materials & Interfaces, 31, (2016), pp. 19872–19882.
[146] A.W. Dunn, S.M. Ehsan, D. Mast, G.M. Pauletti, H. Xu, J. Zhang, et al., Materials Science and Engineering: C, (2015), pp. 97–102.
[147] Z. Zhou, Y. Sun, J. Shen, J. Wei, C. Yu, B. Kong, et al., Biomaterials, 26, (2014), pp. 7470–7478.
[148] E. Alphandéry, Frontiers in bioengineering and biotechnology, (2014), pp. 5.
[149] X. Huang, S. Tang, X. Mu, Y. Dai, G. Chen, Z. Zhou, et al., Nature Nanotechnology, 1, (2011), pp. 28–32.
[150] W. Fang, S. Tang, P. Liu, X. Fang, J. Gong, N. Zheng, Small, 24, (2012), pp. 3816–3822.
[151] C.M. Hessel, V. P. Pattani, M. Rasch, M.G. Panthani, B. Koo, J.W. Tunnell, et al., Nano Letters, 6, (2011), pp. 2560–2566.
[152] Q. Tian, F. Jiang, R. Zou, Q. Liu, Z. Chen, M. Zhu, et al., ACS Nano, 12, (2011), pp. 9761–9771.
[153] Sungjee Kim, Brent Fisher, and Hans-Jürgen Eisler, M. Bawendi*, J. Am. Chem. Soc, 38, (2003), pp. 11466–11467.
[154] J. Wang, S. Han, D. Ke, R. Wang, Journal of Nanomaterials, (2012), pp. 1–8.
[155] X. Gao, Y. Cui, R.M. Levenson, L.W.K. Chung, S. Nie, Nature Biotechnology, 8, (2004), pp. 969–976.
[156] Christian Kirchner, Tim Liedl, Stefan Kudera, Teresa Pellegrino, Almudena Muñoz Javier,

Hermann E. Gaub, et al., Nano Lett, 2, (2005), pp. 331–338.
[157] N. Yin, T. Jiang, J. Yu, J. He, X. Li, Q. Huang, et al., Journal of Nanoparticle Research, 3, (2014), pp. 2306.
[158] W. Ren, Y. Yan, L. Zeng, Z. Shi, A. Gong, P. Schaaf, et al., Advanced Healthcare Materials, 10, (2015), pp. 1526–1536.
[159] Z. Sun, H. Xie, S. Tang, X.-F. Yu, Z. Guo, J. Shao, et al., Angewandte Chemie International Edition, 39, (2015), pp. 11526–11530.
[160] D. Ding, W. Guo, C. Guo, J. Sun, N. Zheng, F. Wang, et al., Nanoscale, 5, (2017), pp. 2020–2029.
[161] H.S. Jang, K. Woo, K. Lim, Optics Express, 15, (2012), pp. 17107.
[162] E.C. Ximendes, U. Rocha, C. Jacinto, K.U. Kumar, D. Bravo, F.J. López, et al., Nanoscale, 5, (2016), pp. 3057–3066.
[163] Z.Q. Li, S. Chen, J.J. Li, Q.Q. Liu, Z. Sun, Z.B. Wang, et al., Journal of Applied Physics, 1, (2012), pp. 014310.
[164] H.K. Dan, D. Zhou, R. Wang, Q. Jiao, Z. Yang, Z. Song, et al., Ceramics International, 2, (2015), pp. 2648–2653.
[165] L. Cheng, C. Wang, Z. Liu, Chinese Journal of Clinical Oncology, 1, (2014), pp. 18–26.
[166] Y. Su, X. Liu, P. Lei, X. Xu, L. Dong, X. Guo, et al., Dalton Transactions, 27, (2016), pp. 11129–11136.
[167] B. Liu, C. Li, P. Yang, Z. Hou, J. Lin, Advanced Materials, 18, (2017), pp. 1605434.
[168] U. Rocha, J. Hu, E.M. Rodríguez, A.S. Vanetsev, M. Rähn, V. Sammelselg, et al., Small, 39, (2016), pp. 5394–5400.
[169] E. Carrasco, B. del Rosal, F. Sanz-Rodríguez, Á.J. de la Fuente, P.H. Gonzalez, U. Rocha, et al., Advanced Functional Materials, 4, (2015), pp. 615–626.
[170] E.C. Ximendes, U. Rocha, C. Jacinto, K.U. Kumar, D. Bravo, F.J. López, et al., Nanoscale, 5, (2016), pp. 3057–3066.
[171] E.C. Ximendes, U. Rocha, K.U. Kumar, C. Jacinto, D. Jaque, Applied Physics Letters, 25, (2016), pp. 253103.
[172] Y. Ito, R.P. Kennan, E. Watanabe, H. Koizumi, Journal of Biomedical Optics, 4, (2000), pp. 383.
[173] N. Shen, C.B. Schaffer, D. Datta, E. Mazur, in: Tech. Dig. Summ. Pap. Present. Conf. Lasers Electro-Optics. Postconf. Tech. Dig. (IEEE Cat. No.01CH37170), IEEE, 2001, pp. 403–404.
[174] R. Hachani, M.A. Birchall, M.W. Lowdell, G. Kasparis, L.D. Tung, B.B. Manshian, et al., Scientific Reports, 1, (2017), pp. 7850.
[175] R. Hachani, M. Lowdell, M. Birchall, A. Hervault, D. Mertz, S. Begin-Colin, et al., Nanoscale, 6, (2016), pp. 3278–3287.
[176] D.H. Ortgies, F.J. Teran, U. Rocha, L. de la Cueva, G. Salas, D. Cabrera, et al., Advanced Functional Materials, (2018), pp. 1704434.
[177] J. Huang, Y. Li, A. Orza, Q. Lu, P. Guo, L. Wang, et al., Advanced functional materials, 22, (2016), pp. 3818–3836.
[178] G. Settanni, J. Zhou, T. Suo, S. Schöttler, K. Landfester, F. Schmid, et al., Journal of Materials Chemistry C, (2015), pp. 1–3.
[179] V.H. Nguyen, B.-J. Lee, International journal of nanomedicine, (2017), pp. 3137–3151.
[180] M. Bednarski, M. Dudek, J. Knutelska, L. Nowiński, J. Sapa, M. Zygmunt, et al.,

Pharmacological Reports, 3, (2015), pp. 405–409.
[181] R.R. Arvizo, O.R. Miranda, D.F. Moyano, C.A. Walden, K. Giri, R. Bhattacharya, et al., PLoS ONE, 9, (2011), pp. e24374.
[182] R. Lehner, X. Wang, S. Marsch, P. Hunziker, Nanomedicine: Nanotechnology, Biology and Medicine, 6, (2013), pp. 742–757.
[183] I. Fratoddi, I. Venditti, C. Cametti, M.V. Russo, Nano Research, 6, (2015), pp. 1771–1799.
[184] N. Khlebtsov, L. Dykman, Chemical Society reviews, 3, (2011), pp. 1647–71.
[185] U. Patil, S. Adireddy, A. Jaiswal, S. Mandava, B. Lee, D. Chrisey, International Journal of Molecular Sciences, 12, (2015), pp. 24417–24450.
[186] N. Singh, G.J.S. Jenkins, R. Asadi, S.H. Doak, Nano reviews, (2010),.
[187] S. Shen, F. Kong, X. Guo, L. Wu, H. Shen, M. Xie, et al., Nanoscale, 17, (2013), pp. 8056–8066.
[188] S.J.H. Soenen, M. De Cuyper, Contrast Media & Molecular Imaging, 5, (2009), pp. 207–219.
[189] K. Parivar, F. Malekvand Fard, M. Bayat, S.M. Alavian, M. Motavaf, Iranian Red Crescent medical journal, 1, (2016), pp. e28939.
[190] H. Arami, A. Khandhar, D. Liggitt, K.M. Krishnan, Chemical Society reviews, 23, (2015), pp. 8576–607.
[191] K. Dassler, J. Roohi, A. Lohrke, G. Ide, K. Schuetz, International Journal of Nanomedicine, (2012), pp. 4447.
[192] O. Ziv-Polat, M. Topaz, T. Brosh, S. Margel, Biomaterials, 4, (2010), pp. 741–747.
[193] L. Yang, H. Kuang, W. Zhang, Z.P. Aguilar, Y. Xiong, W. Lai, et al., Nanoscale, 2, (2015), pp. 625–636.
[194] J. Schuemann, R. Berbeco, D.B. Chithrani, S.H. Cho, R. Kumar, S.J. McMahon, et al., International Journal of Radiation Oncology*Biology*Physics, 1, (2016), pp. 189–205.
[195] R.A. Kudgus, C.A. Walden, R.M. McGovern, J.M. Reid, J.D. Robertson, P. Mukherjee, Scientific reports, 1, (2014), pp. 5669.
[196] M.R.K. Ali, M.A. Rahman, Y. Wu, T. Han, X. Peng, M.A. Mackey, et al., Proceedings of the National Academy of Sciences, 15, (2017), pp. E3110–E3118.
[197] X. Li, Z. Hu, J. Ma, X. Wang, Y. Zhang, W. Wang, et al., Colloids and Surfaces B: Biointerfaces, (2018), pp. 260–266.
[198] S. Nahle, R. Safar, S. Grandemange, B. Foliguet, M. Lovera-Leroux, Z. Doumandji, et al., Journal of Applied Toxicology, (2019),.
[199] P. Southern, Q.A. Pankhurst, International Journal of Hyperthermia, 6, (2018), pp. 671–686.
[200] A. Espinosa, J. Kolosnjaj-Tabi, A. Abou-Hassan, A. Plan Sangnier, A. Curcio, A.K.A. Silva, et al., Advanced Functional Materials, 37, (2018), pp. 1803660.
[201] C. Chen, S. Wang, L. Li, P. Wang, C. Chen, Z. Sun, et al., Biomaterials, (2016), pp. 352–360.
[202] E.B. Dickerson, E.C. Dreaden, X. Huang, I.H. El-Sayed, H. Chu, S. Pushpanketh, et al., Cancer Letters, 1, (2008), pp. 57–66.
[203] X. Ding, R. Singh, A. Burke, H. Hatcher, J. Olson, R.A. Kraft, et al., Nanomedicine, 8, (2011), pp. 1341–1352.
[204] S. Wilhelm, A.J. Tavares, Q. Dai, S. Ohta, J. Audet, H.F. Dvorak, et al., Nature Reviews Materials, 5, (2016), pp. 16014.

[205] M.W. Dewhirst, C.T. Lee, K.A. Ashcraft, International Journal of Hyperthermia, 1, (2016), pp. 4–13.
[206] M. Moros, J. Idiago-López, L. Asín, E. Moreno-Antolín, L. Beola, V. Grazú, et al., Adv. Drug Deliv. Rev. 138, (2019), pp.326–343.
[207] J.C. Bear, P.S. Patrick, A. Casson, P. Southern, F.Y. Lin, M.J. Powell, et al., Scientific Reports, (2016),.
[208] L. Che Rose, J.C. Bear, P. Southern, P.D. McNaughter, R. Ben Piggott, I.P. Parkin, et al., Journal of Materials Chemistry B, 9, (2016), pp. 1704–1711.
[209] M.D. Norris, K. Seidel, A. Kirschning, Advanced Therapeutics, 1, (2019), pp. 1800092.
[210] B.L. Caetano, C. Guibert, R. Fini, J. Fresnais, S.H. Pulcinelli, C. Ménager, et al., RSC Advances, 68, (2016), pp. 63291–63295.
[211] S. Shen, D. Huang, J. Cao, Y. Chen, X. Zhang, S. Guo, et al., Journal of Materials Chemistry B, 7, (2019), pp. 1096–1106.
[212] X. Wu, J. Liu, L. Yang, F. Wang, Colloids and surfaces. B, Biointerfaces, (2019), pp. 239–247.
[213] A.R. Guerrero, N. Hassan, C.A. Escobar, F. Albericio, M.J. Kogan, E. Araya, Nanomedicine 9, (2014), pp.2023–2039.
[214] H. Peinado, H. Zhang, I.R. Matei, B. Costa-Silva, A. Hoshino, G. Rodrigues, et al., Nature Reviews Cancer, 5, (2017), pp. 302–317.
[215] J.W. Ivey, M. Bonakdar, A. Kanitkar, R. V. Davalos, S.S. Verbridge, Cancer Letters, 1, (2016), pp. 330–339.
[216] E. Ju, K. Dong, Z. Liu, F. Pu, J. Ren, X. Qu, Advanced Functional Materials, 10, (2015), pp. 1574–1580.
[217] J. Kolosnjaj-Tabi, I. Marangon, A. Nicolas-Boluda, A.K.A. Silva, F. Gazeau, Pharmacological Research, (2017), pp. 123–137.
[218] R. Tong, R. Langer, The Cancer Journal, 4, (2015), pp. 314–321.
[219] J. Kolosnjaj-Tabi, R. Di Corato, L. Lartigue, I. Marangon, P. Guardia, A.K.A. Silva, et al., ACS Nano, 5, (2014), pp. 4268–4283.
[220] E. Blanco, H. Shen, M. Ferrari, Nature Biotechnology, 9, (2015), pp. 941–951.
[221] M. Yu, J. Zheng, ACS Nano, 7, (2015), pp. 6655–6674.
[222] B. Albertini, V. Mathieu, N. Iraci, M. Van Woensel, A. Schoubben, A. Donnadio, et al., Molecular Pharmaceutics, 6, (2019), pp. 2430–2444.
[223] A. Agarwal, S.W. Huang, M. O'Donnell, K.C. Day, M. Day, N. Kotov, et al., Journal of Applied Physics, 6, (2007),.
[224] C.J. Legge, H.E. Colley, M.A. Lawson, A.E. Rawlings, Journal of Oral Pathology & Medicine, (2019), pp. jop.12921.
[225] J. Shi, P.W. Kantoff, R. Wooster, O.C. Farokhzad, Nature Reviews Cancer, 1, (2017), pp. 20–37.
[226] Y.-H. Wang, S.-P. Chen, A.-H. Liao, Y.-C. Yang, C.-R. Lee, C.-H. Wu, et al., Scientific Reports, 1, (2015), pp. 5685.
[227] L. Zou, H. Wang, B. He, L. Zeng, T. Tan, H. Cao, et al., Theranostics, 6, (2016), pp. 762–72.
[228] G. Kandasamy, D. Maity, International Journal of Pharmaceutics, 2, (2015), pp. 191–218.
[229] N.V.S. Vallabani, S. Singh, 3 Biotech, 6, (2018), pp. 279.
[230] K. Maier-Hauff, F. Ulrich, D. Nestler, H. Niehoff, P. Wust, B. Thiesen, et al., Journal of

neuro-oncology, 2, (2011), pp. 317–24.
[231] J.P. Bullivant, S. Zhao, B.J. Willenberg, B. Kozissnik, C.D. Batich, J. Dobson, International journal of molecular sciences, 9, (2013), pp. 17501–10.
[232] Y.-X.J. Wang, World journal of gastroenterology, 47, (2015), pp. 13400–2.
[233] A.C. Anselmo, S. Mitragotri, The AAPS Journal, 5, (2015), pp. 1041–1054.

## Authors' Biography

Dr. **Surender Kumar Sharma** is a faculty in Materials Science at Department of Physics, Faculty of Science & Technology, The University of the West Indies (UWI), Trinidad & Tobago. Before joining UWI, he worked as a Professor Adjunto (IV) at Department of Physics, Federal University of Maranhão (UFMA), Brazil (2014-2019). He has received his Ph.D. in Physics from Himachal Pradesh University, Shimla, India in 2007. He worked on different research/academic positions in Brazil, France, Czech Republic, India and Mexico from 2007-2014. His research interests include magnetic nanohybrids, their synthesis, characterization and utilization in magnetic and biomedical applications.

**Navadeep Shrivastava** has obtained his Ph.D. from Federal University of Maranhão, Brazil under guidance of Prof. Dr. Surender Kumar Sharma in 2017. He majored in Mathematics and Physics in his Bachelor of Science (2010) and Master of Science in Physics (2013) from University of Allahabad, India. During his Ph.D., he worked on hybrid magnetic-luminescent nanomaterials and their application in radiation detection. His expertise lies in the syntheses and characterizations of multifunctional nanomaterials based on magnetic nanoparticles and rare-

earth spectroscopy. Currently, he is involved in research activities as a Post-Doctoral Researcher, at Institute of Physics, Federal University of Goiás, Brazil with a major research focus in design of multifunctional colloidal nanohybrids for thermal nanomedicine, multimodal imaging and nanothermometry.

**Francesco Rossi** is a PhD student of the Biophysics Group at the Department of Physics and Astronomy at UCL. He achieved is BSc and MSc at the university of Florence (Italy) and spent two years working as laboratory technician for Procarta Biosystems (UK) and participated at the A*STAR exchange project between UCL and IMRE of Singapore from 2016 to 2018. His research consists of developing anisotropic nanomaterials able to interact with light. Light activated particles can be used to create auto sterilizing polymers to be used in medical and food industry.

**Le Duc Tung** received his Ph.D. degree in Physics from University of Amsterdam in 1998. He was a postdoctoral fellow at the University of New Orleans (2001-2003), University of Warwick (2003-2007), University of Liverpool (2007-2010). Currently he is a senior research fellow at Biophysics Group, Department of Physics & Astronomy, University College London. His research

interests are in magnetism and magnetic materials and recently focused on biomedical applications of magnetic nanoparticles.

Professor **Nguyen T. K. Thanh**, FRSC FIMMM FInstP FRSB (http://www.ntk-thanh.co.uk) held a prestigious Royal Society University Research Fellowship (2005-2014) and was promoted to full professor of nanomaterials in 2013 at University College London. She conducts cutting edge interdisciplinary and innovative research on the design, chemical synthesis, physical characterization of magnetic and plasmonic nanomaterials for biomedical applications. In collaboration with physicists, material scientists, chemical engineers she has produced the next generation of nanoparticles with very high magnetic moment, fine tuning Au nanorods, novel hybrid and multifunctional nanostructures. Detailed mechanistic studies of their formation by sophisticated and advanced analysis of the nanostructure allows tuning of the physical properties at the nanoscale; these can subsequently be exploited for diagnosis and treatment of various diseases in collaboration with biologists, biochemists and clinicians. She has published over 100 peer reviewed journal articles and book chapters, books and theme issues. Among them 9 papers were featured as cover pages. Her research has accrued ~6000 citations, with an average 64 citation per item, giving her an i10 of 50, and notably she has 10 papers with over 100 citations, with 1 research paper attracting an exceptional 1500 citations.